

AD719891

NAVAL SHIP RESEARCH AND DEVELOPMENT CENTER

Washington, D. C. 20034

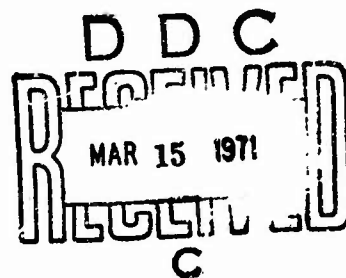


FLUTTER AND DIVERGENCE CHARACTERISTICS
OF FOUR LOW MASS RATIO HYDROFOILS

by

Peter K. Besch
and
Yuan-Ning Liu

Approved for public release:
Distribution Unlimited



SHIP PERFORMANCE DEPARTMENT
RESEARCH AND DEVELOPMENT REPORT

January 1971

Report 3410

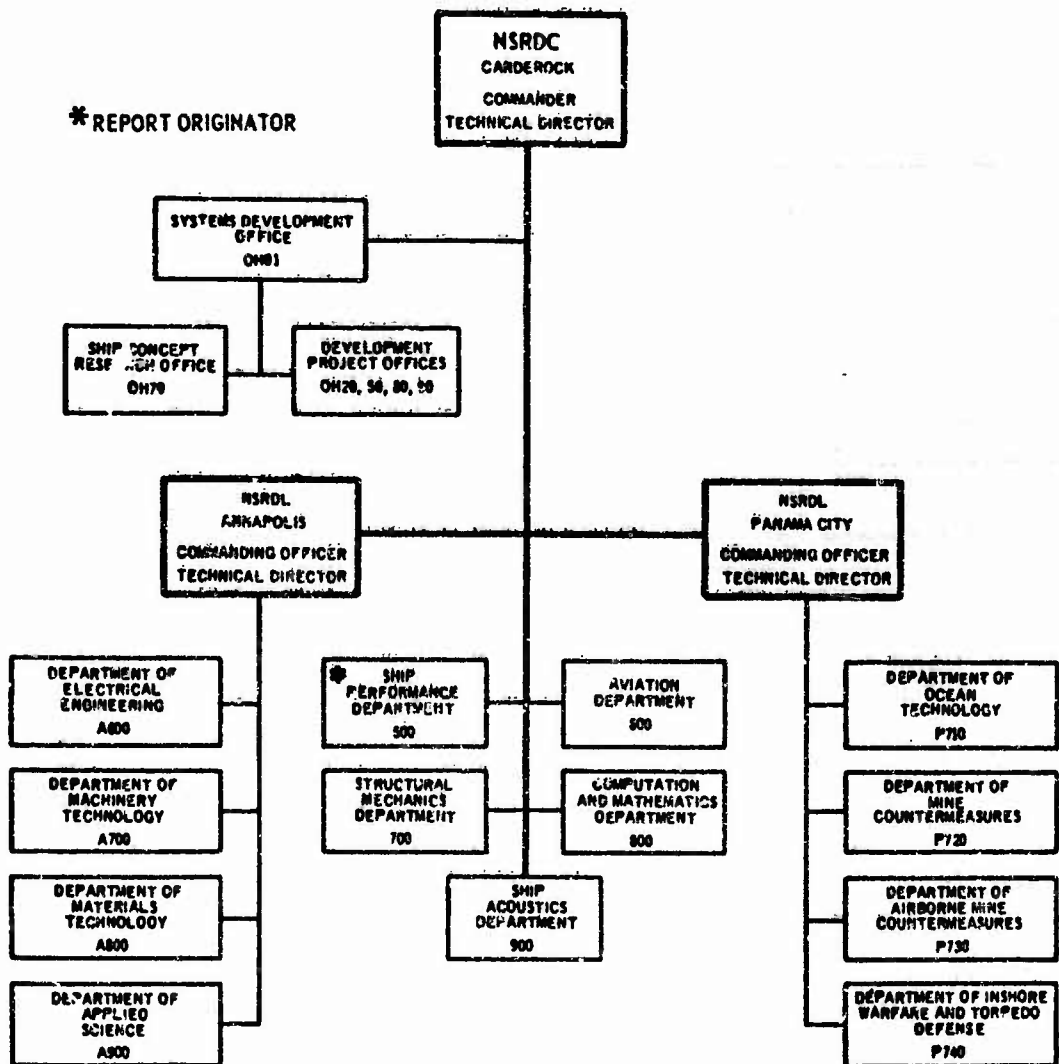
Reproduced by
NATIONAL TECHNICAL
INFORMATION SERVICE
Springfield, Va. 22151

ACCESSION NO.	
DPSTI	WHITE SECTION <input checked="" type="checkbox"/>
NSC	BUFF SECTION <input type="checkbox"/>
UNANNOUNCED	<input type="checkbox"/>
JUSTIFICATION	
BY	
DISTRIBUTION/AVAILABILITY CODES	
DIST.	AVAIL. AND/OR SPECIFIC
A	

The Naval Ship Research and Development Center is a U.S. Navy center for laboratory effort directed at achieving improved sea and air vehicles. It was formed in March 1967 by merging the David Taylor Model Basin at Carderock, Maryland and the Marine Engineering Laboratory (now Naval Ship R & D Laboratory) at Annapolis, Maryland. The Mine Defense Laboratory (now Naval Ship R & D Laboratory) Panama City, Florida became part of the Center in November 1967.

Naval Ship Research and Development Center
Washington, D. C. 20034

MAJOR NSRDC ORGANIZATIONAL COMPONENTS



DEPARTMENT OF THE NAVY
NAVAL SHIP RESEARCH AND DEVELOPMENT CENTER
WASHINGTON, D. C. 20034

FLUTTER AND DIVERGENCE CHARACTERISTICS
OF FOUR LOW MASS RATIO HYDROFOILS

by

Peter K. Besch
and
Yuan-Ning Liu

Approved for public release:
Distribution Unlimited

January 1971

Report 3410

TABLE OF CONTENTS

	Page
ABSTRACT.....	1
ADMINISTRATIVE INFORMATION.....	1
INTRODUCTION	1
FLUTTER MODELS	2
MODEL SUPPORT SYSTEM.....	3
PROCEDURE	4
STIFFNESS MEASUREMENTS.....	4
STRUCTURAL MODE MEASUREMENTS.....	5
FLUTTER TESTING.....	5
RESULTS	7
STIFFNESSES	7
STRUCTURAL MODES.....	7
FLUTTER CHARACTERISTICS.....	8
THEORETICAL FLUTTER ANALYSIS.....	10
YATES FLUTTER THEORY	10
NSRDC FLUTTER THEORY.....	12
SwRI FLUTTER THEORY	13
DISCUSSION	13
THEORETICAL DIVERGENCE ANALYSIS.....	14
CONCLUSIONS.....	17
RECOMMENDATIONS.....	18
PERSONNEL AND ACKNOWLEDGMENTS	18
REFERENCES.....	40

LIST OF FIGURES

	Page
Figure 1 – Spar and Ballasted Segments before Assembly	19
Figure 2 – Completed Models	20
Figure 3 – Flutter Model and Model Support Enclosure Mounted in 36-Inch Variable Pressure Water Tunnel	21
Figure 4 – Section through Turntable	22
Figure 5 – Excitation of Flutter Model by Electromagnetic Oscillation	23
Figure 6 – Theoretical and Experimental Nodal Lines for the First Six Natural Frequencies of Flutter Models in Air	24
Figure 7 – Model 2 after Static Failure in Bending	26
Figure 8 – Exponential Decay Factor δ as a Function of Speed for Model 1	27
Figure 9 – Frequency as a Function of Speed for Model 1	27
Figure 10 – Exponential Decay Factor δ as a Function of Speed for Model 2	28
Figure 11 – Frequency as a Function of Speed for Model 2	28
Figure 12 – Exponential Decay Factor δ as a Function of Speed for Model 4	29
Figure 13 – Frequency as a Function of Speed for Model 4	29
Figure 14 – Spanwise Load Distributions for Aspect Ratio 5 Rectangular Foil	30
Figure 15 – Exponential Decay Factor δ as a Function of Speed for Model 3	30
Figure 16 – Frequency as a Function of Speed for Model 3	31
Figure 17 – Exponential Decay Factor δ as a Function of Speed for the SwRI 30-Inch Flutter Model	32
Figure 18 – Frequency as a Function of Speed for the SwRI 30-Inch Flutter Model	32
Figure 19 – Noncirculatory Modification Factor p as a Function of Spanwise Position for an Aspect Ratio 5 Hydrofoil	33

	Page
Figure 20 – Theoretical and Experimental Flutter Speeds for Models 1–4 as a Function of Mass Ratio	33
Figure 21 – Foil Deflection Angles	33
Figure 22 – Ratio of Angle of Twist at Tip to Uniform Misalignment Angle as a Function of Speed for Model 2.....	34
Figure 23 – Misalignment Angle γ to Cause Spar Failure in Bending for Model 2 as a Function of Speed.....	34
Figure 24 – Theoretical Divergence Speed as a Function of Elastic Axis Position for Model 2	35

LIST OF TABLES

Table 1 – Structural Parameter Values for the Flutter Models.....	36
Table 2 – Theoretical and Experimental Natural Frequencies for SwRI 30-Inch Parent Model	36
Table 3 – Theoretical and Experimental Natural Frequencies for Model 1	37
Table 4 – Theoretical and Experimental Natural Frequencies for Model 2	37
Table 5 – Theoretical and Experimental Natural Frequencies for Model 3	38
Table 6 – Theoretical and Experimental Natural Frequencies for Model 4	38
Table 7 – Measured Structural Damping ζ_s for Flutter Models.....	39

NOTATION

Symbol	Definition
a	Distance of pitch axis from midchord of hydrofoil model, in units of semichord (positive aft)
A^*	Local aspect ratio; square of distance from local position to tip of hydrofoil divided by one-half the area from local position to tip of hydrofoil
b	Semichord of hydrofoil model
EI	Bending stiffness
GJ	Torsional stiffness
h_i	Translation of foil elastic axis from unstressed position at station i
k	Reduced frequency; $b\omega/V$
$[K_h]$	Bending stiffness matrix
$[K_\theta]$	Torsional stiffness matrix
L	Length of hydrofoil from root to tip
$M_0(\alpha_i)$	Steady moment on foil due to angle of attack at station i
p	Spanwise modification factor for noncirculatory loading
$P_0(\alpha_i)$	Steady lift on foil due to angle of attack at station i
r_G	Radius of gyration, in units of semichord
t	Time
U_D	Divergence speed of foil
V	Water speed
x_G	Distance of center of gravity from elastic axis, in units of semichord (positive aft)
α_i	Angle of attack of foil relative to free stream at station i
γ_i	Angle of unstressed foil relative to free stream at station i
δ	Exponential decay factor corresponding to oscillation of amplitude proportional to $e^{-\delta t}$

Symbol	Definition
δ_h	Component of exponential decay factor due to hydrodynamic damping
δ_s	Component of exponential decay factor due to structural damping: $\zeta_s \sqrt{\omega^2 + \delta_h^2}$
ζ_s	Structural damping parameter
θ_i	Torsional displacement of foil elastic axis from unstressed position at station i
μ	Mass ratio; ratio of mass of hydrofoil to mass of cylinder of water circumscribing chord of foil
ω	Circular frequency of oscillation

ABSTRACT

Four low mass ratio hydrofoil models of aspect ratio 5 were flutter tested. The flutter speed of the mass ratio 0.963 model was 24.7 knots. The other three models, of mass ratios 0.455, 0.395, and 0.202, were subject to static failure in bending at about 36 knots and did not flutter below this speed. The results were compared with the predictions of three flutter theories. All theories gave conservative flutter speed predictions at mass ratio 0.963. Two of the theories were also conservative at mass ratio 0.455. The other predictions could not be evaluated. Model divergence characteristics were responsible for model failure in bending.

ADMINISTRATIVE INFORMATION

The work performed at the Naval Ship Research and Development Center was funded by the Naval Ship Systems Command under Subproject S4606, Task 1703.

The work performed at Southwest Research Institute was sponsored by the Hydro-mechanics Laboratory of the Naval Ship Research and Development Center under the Naval Ship Systems Command Subproject S4606, Task 1703. Funding was provided according to Contract N00014-69-C-0219.

INTRODUCTION

A long-standing difficulty in the field of hydrofoil flutter research has been the inability of flutter theory and experiment to establish the dependence of hydrofoil flutter characteristics on mass ratio in the mass ratio range below 1.0. While flutter theory has generally failed to predict experimental results,^{1, 2, 3} flutter experiments as well have often failed to produce usable results in the form of flutter occurrences.^{4, 5} In cases where some agreement has been obtained between theory and experiment, the data have been insufficient to confirm theoretical predictions over a range of mass ratio values⁶ and the theories have lacked general applicability³ or self-consistency.¹

A study by Rowe³ using highly accurate structural calculations indicated that the deficiencies of flutter theory lay in the hydrodynamic loading formulation. By using an improved aerodynamic strip theory in a six-mode Rayleigh-type analysis, Yates⁷ successfully predicted the flutter characteristics of airfoils of mass ratio as low as 1.0 and obtained results within 20 percent of experiment for a hydrofoil⁸ of mass ratio 0.99. Yates also predicted a flutter boundary at very low mass ratio, characterized by a flutter speed which approached zero as mass ratio approached zero. The existence of such a flutter boundary would be highly significant for full-scale hydrofoils.

¹References are listed on page 40.

It was felt that Yates' flutter theory was a significant improvement over existing flutter theories in its modification of two-dimensional strip theory to include three-dimensional effects on loading. However, additional data were required to confirm its predictions of flutter at low mass ratio. Therefore the present work was undertaken.

Four hydrofoil flutter models, and a model support system, were designed and constructed by Southwest Research Institute (SwRI).⁹ The flutter models ranged in mass ratio from 0.963 to 0.202, with the 0.963 model being a dynamically scaled model of the mass ratio 0.99 hydrofoil mentioned above. The models were flutter tested in the 36-in. variable pressure water tunnel¹⁰ at the Naval Ship Research and Development Center (NSRDC) during February 1970.

The flutter characteristics of the four flutter models were calculated using three flutter theories. Each of the flutter theories incorporated some spanwise modification of hydrodynamic loading, but none was precisely the same as Yates' original calculation. In a calculation made at NSRDC, Yates' loading was combined with a lumped parameter structural representation similar to Rowe. Second, the load theory was extended, as suggested by Yates,⁷ to include three-dimensional effects on noncirculatory loading and was used with the lumped parameter structural representation. The third calculation, performed at SwRI, used measured values of spanwise lift slope in a two-mode Rayleigh-type analysis.¹¹ Results calculated for the mass ratio 0.99 hydrofoil by the two NSRDC theories are also presented. Results for this hydrofoil calculated by the SwRI theory have been previously published.¹¹

FLUTTER MODELS

Model design and construction have been fully described in a previous report.⁹ The following discussion is intended as a summary of model design philosophy and characteristics.

The four flutter models were intended to form a family in which mass ratio varied to substantially below 1.0 while all other parameters remained constant. Geometrical size and design flutter speeds were based on the capabilities of the test facility, the 36-in. variable pressure water tunnel¹⁰ at NSRDC. A parent model which had been previously flutter tested⁸ provided values for the invariant structural parameters and for the mass ratio of the heaviest of the new models (Model 1). This correlation permitted a comparison of scaling effects between the parent model and the new, smaller Model 1. The remaining models, Models 2, 3, and 4, were of lower mass ratio than Model 1.

The parent model was an aspect ratio 5 rectangular hydrofoil with a 30-in. span (to a reflecting plate) and a mass ratio of 0.99. It had undergone structural failure after flutter occurred at 48.1 knots, with a frequency of 17.5 Hz and a reduced frequency of 0.676. In order to preserve similarity between the hydrodynamic forces acting on the parent and Model 1, the same value of reduced frequency at flutter was sought for Model 1. The 50-knot maximum speed of the water tunnel and its 36-in. diameter jet led to a choice of $b_{\text{Model 1}} = 1/2 b_{\text{Parent}}$ and $k_{\text{Model 1}} = k_{\text{Parent}}$, which would hopefully result in the relationship $V_{\text{Model 1}} = 1/2 V_{\text{Parent}}$ at flutter. These scale ratios gave a wide speed range for testing, enabled the resulting

15-in. models and a reflecting plate to be located well inside the water jet, and represented feasible structural stiffnesses with EI and GJ being $1/64$ of the parent model values. The structural parameter values of the parent model are given in Table 1.

The models were constructed by cementing airfoil-shaped segments to steel spars at the quarter chord position. The segments were ballasted to produce the desired inertial characteristics. Four identical spars were manufactured from high strength maraging steel with a yield point of 350,000 psi. Segments were individually cast of the following materials to produce the desired variation in mass ratio:

Model	Segment Material
1	73 percent lead, 27 percent tin
2	epoxy and lead powder
3	epoxy and lead powder
4	epoxy and glass microballoons

One of the models is shown in Figure 1 prior to assembly. Each model contained an exciter rod anchored to its spar tip, passing through the center of the spar, and extending beyond the root end of the spar. Strain gages sensitive to bending and torsion were cemented to the root of the spar in a hollowed-out portion of the root segment. After assembly, gaps between segments were sealed with Silastic RTV 731 compound to form a smooth surface. Two of the completed models are shown in Figure 2.

Inertial parameter values for the completed models are given in Table 1, along with the values for the parent model. Values of mass unbalance x_{α} and radius of gyration r_{α} agreed extremely well with design values. The mass ratio of Model 1 was slightly below the intended value of 0.99, while the mass ratio of Model 4 was the lowest obtainable with available materials.

MODEL SUPPORT SYSTEM

Each model was supported for flutter testing by an enclosure which was bolted to the ceiling of the water tunnel, as shown in Figure 3. The bottom of the enclosure consisted of a reflection plate 40 in. long and 24 in. wide the upper surface of which was bevelled. The reflection plate extended 3 in. into the water jet, and the model extended 15 in. further to the centerline of the water jet. The enclosure had an NACA 16-022 profile.

Within the enclosure were housed mechanisms for adjusting the angle of attack, or trim, of the flutter model and for twisting the exciter rod in the model to produce a tip deflection. The model was clamped in a turntable mounted flush with the bottom of the reflection plate, as shown in Figure 4. Trim adjustment was made by rotating the entire turntable and retainer plate assembly on Teflon coated surfaces. The exciter rod was twisted by a cam acting on the exciter crank independently of the turntable, allowing the tip deflection to be released quickly

after reaching its maximum. By operating the cam drive motor both clockwise and counter-clockwise, two tip deflection amplitudes were obtained. Initially the deflections were 5 deg and 2 deg. During the test, the cam was machined down to give deflections of 2 deg and 2/3 deg.

This method of deflecting and releasing the model has been previously used to measure damping in a hydrofoil flutter test.⁸ However, the hydrofoil in that test was destroyed when flutter occurred. It was felt that flutter of the present models could be avoided by testing until damping had become very small and then removing the models from the water tunnel. The flutter inception speed would be determined by extrapolation to zero damping.

PROCEDURE

STIFFNESS MEASUREMENTS

Bending and torsional stiffness measurements were made prior to flutter testing on all four models and were repeated on the three surviving models after flutter testing. Pre-test measurements were made with each model clamped in a vise, while post-test measurements were made with each model fixed in the model support enclosure which was used during flutter testing.

The models were statically deflected in bending or torsion in the following manner. Bolts were placed in threaded holes in the tip of the model, one in the center of the spar and the other 2 in. aft of the spar center. Bending deflections were produced by applying loads at the spar tip perpendicular to the foil planform. A dial gage read deflections at the spar. Torsional deflections were produced by placing a knife-edged bolt in the spar tip and applying loads to the other bolt while the knife edge rested on a support. A maximum of 15 lb of weights was used to load the models.

Bending stiffness EI was calculated from the relation¹²

$$EI = \frac{P}{y} \left(\frac{Lx^2}{2} - \frac{x^3}{6} \right)$$

where P = force applied to tip of spar,

y = spar deflection at spanwise position x ,

L = length of spar, and

x = spanwise position at which deflection is measured.

This relation is based on the assumption that EI is constant along the spar. The torsional stiffness GJ was calculated from the relation¹³

$$GJ = \frac{Mx}{\theta}$$

where M = moment applied to tip of spar,

x = spanwise position at which twist angle is measured, and

θ = twist angle at spanwise position x .

It is assumed that GJ is constant along the spar.

STRUCTURAL MODE MEASUREMENTS

The two lowest natural frequencies of the parent model were determined by tip excitation at the time of its flutter testing. The frequencies in air and in water are given in Table 2.

The natural frequencies and some nodal lines for the current models were obtained by exciting each model with an electromagnetic shaker placed about 1/4 in. from the surface of the model, over the spar and near the model's tip, as shown in Figure 5. There was no mechanical connection between the model and the shaker. The shaker was driven by a sweep oscillator which automatically varied its frequency over a preset range. Model response was registered by an accelerometer taped to the model on the opposite side from the shaker. Acceleration amplitude was automatically plotted as a function of frequency, with resonant frequencies corresponding to response peaks. A second "roving" accelerometer was used to determine the mode shape by locating nodal lines. Crossing a nodal line resulted in a 180-deg phase change between the two accelerometer signals.

Structural damping in the form of the damping constant ζ_s for the models was obtained in two ways. In the first method, it was assumed that the amplitude of decaying oscillations was proportional to $e^{-\zeta_s \omega t}$. The constant ζ_s was determined directly from the oscillations recorded after the tip of the model was twisted and released. The second method involved calculation of ζ_s from the width of the model response curve at a resonant frequency.¹⁴

FLUTTER TESTING

Flutter testing of the four hydrofoil models was performed in the 36-in. variable pressure water tunnel at NSRDC. The maximum speed through the test section is 50 knots. Static pressure at the test section centerline can be varied from 4 to 60 psia.

The model support enclosure was mounted in the ceiling of the open jet test section, as shown in Figure 3, with the model extending to the centerline of the test section.

After installation in the tunnel, the strain gages in each model were connected to Endevco Model 4402 signal conditioning units. Gage output was amplified by Dana Model 282J amplifiers and recorded on a Consolidated Electrodynamics Corporation Model 5-124 oscillograph. The model was excited in air in order to obtain structural damping values for the two lowest modes.

Since both the enclosure and the model were hollow, it was decided to maintain a slightly higher air pressure inside them than in the test section to prevent water from entering.

This pressure differential had to be maintained throughout an absolute pressure range of about 9 to 40 psia which occurred during filling and emptying the tunnel. Following the test-section pressure at all times would also prevent possible damage due to pressure loading on the enclosure and the model. A pressure regulation system was constructed, using a back-pressure regulator containing a teflon diaphragm as the controlling element. High pressure air was bled through the regulator which maintained the desired pressure differential by balancing the tunnel pressure against the enclosure pressure.

During tunnel operation, air constantly leaked out of the enclosure along welded seams which had not been completely filled. Air leaks also occurred from the Silastic seams in Flutter Model 4, because lubricating oil from the exciter rod bearing saturated the inside of the model and gradually loosened the Silastic bonding. Several repairs were made to the seals in order to complete testing Model 4. Air leaks from the enclosure resulted in a continually increasing air content in the tunnel, primarily evidenced by bubbles. High bubble content might affect hydrodynamic loading in addition to reducing visibility. Since the test section was emptied each day, air accumulated for a maximum of seven hours while testing, although running times between refillings were often much less than seven hours. No estimate of the effect of air accumulation could be made from the test data obtained. Some reduction in the quantity of air bubbles was achieved by increasing the static pressure in the tunnel from 20 psia which was used at lower speeds to 25 psia and 30 psia for higher speed runs. The higher pressures also reduced a small amount of cavitation which occurred along the leading edge of the reflection plate.

Flutter testing was performed by increasing the water speed from zero and measuring the model's damping at each speed selected. After zeroing its angle of attack, the model was excited using the internal exciting mechanism. The exponential decay factor δ was then calculated from the recorded signal. Flutter would occur at $\delta = 0$ so that a decrease in δ toward zero would indicate the approach of a flutter instability. This method successfully detected the approach of flutter for Model 1, which was removed from the tunnel intact after coming within an estimated 1/2 knot of flutter. It was found helpful in the low damping range near flutter to make several damping measurements so that data scatter would include the lowest damping value.

Of the two excitation amplitudes available, the high-amplitude excitation was used for low speeds and the low-amplitude for high speeds. The amplitude was reduced when torsional deflection of the model appeared to be too large. Model 1 was tested at 5 deg excitation up to 17 knots, and at 2 deg excitation up to its maximum speed of 24.2 knots. Models 2 and 4 required a reduction in amplitude to 2/3 of a degree for speeds above 30 knots. The reduced amplitude was obtained by machining down the exciter cam. It was found, however, that the 2/3 deg excitation did not give a sufficiently large torsional deflection for the damping to be found. This difficulty appeared to be related to the divergence characteristics of the models as will be discussed elsewhere.

Several excitation responses of the models were recorded on high-speed motion picture film, taken at 500 frames/sec. The camera photographed the motion of the tip of the model from below the tunnel test section.

RESULTS

STIFFNESSES

Bending and torsional stiffness values are given in Table 1, along with the other structural parameters. Values measured after the flutter test agreed with those measured before the test. The values given correspond to model loading in the high load range, around 15 lb, rather than the low load range. Higher loading gave lower stiffnesses because the structural response was nonlinear. The hysteresis curve of the model for cyclic loading was approximately represented by the chosen stiffnesses.

The design values for EI and GJ were 53,100 lb-in.² and 15,200 lb-in.², respectively. Therefore Models 2, 3, and 4 were in good agreement with the design values, while Model 1 exhibited a torsional stiffness which was somewhat high.

STRUCTURAL MODES

The hydrofoils exhibited structural vibration modes which contained both bending and torsion components. However, the two lowest modes were observed to be primarily first bending and first torsion modes, respectively.

Measured natural frequencies are given in Tables 3 through 6. All frequencies up to approximately 200 Hz were determined by forced oscillation, using an electromagnetic shaker, but only the first two modes could be excited by tip excitation. Model 3 was not installed in the tunnel and therefore no tip excitation frequencies are available. The strain gage designed for bending on Model 4 contained a broken lead wire so that no bending frequencies could be obtained. The frequencies obtained by the two methods of excitation agreed within the experimental uncertainty of four percent for mode 1, but did not agree for mode 2 of Models 1 and 2.

A comparison of the natural frequencies for Model 1 and the parent model showed that Model 1 had frequencies which were 15 percent and 7 percent higher than the parent model in modes 1 and 2, respectively. The higher frequencies were due to the relatively higher stiffnesses of Model 1, given in Table 1, which exceeded the stiffness scaling ratio of 1/64. Therefore Model 1 was not a perfectly scaled version of the parent model, and was not expected to have the design flutter characteristics of a 24.05 knot flutter speed and a 17.5 Hz flutter frequency. However, the model was a close approximation to the desired scaling.

Nodal lines obtained during forced oscillation are shown by the data points in Figure 6. The points represent a 180-deg phase change in acceleration. Theoretical nodal lines are also shown in Figure 6 and will be discussed later. The nodal lines for Mode 1, primarily first bending, could not be detected along the roots of the models. Modes 2 and 3 were measured

on each model except Model 3, for which the nodal line of mode 3 could not be detected. The nodal lines were generally smooth curves showing only slight changes from model to model. Mode 2 of Model 4, however, contained an irregularity between the 6th and 7th segments from the tip.

Structural damping values, obtained from tip excitation in air and in water and from the forced oscillation response curves,¹⁴ are given in Table 7. The torsional damping of Model 4 in air could not be determined because the torsion gage output contained too large a bending component.

The two methods of measuring damping did not agree, although damping values obtained by either method were fairly consistent. An evaluation of the experimental uncertainty in the two methods indicated that there was considerably more uncertainty in the damping obtained from forced oscillation response peaks. The uncertainty originated in plotting and measuring the response peak heights and widths, and in possible variation in the driving force of the oscillator as the model response varied. Since damping values obtained from twisting and releasing the models were considered more accurate, these values, taken from in-water model excitation, were used in the flutter calculations. In view of the agreement in measured in-air damping between Models 2 and 3, the in-water damping of Model 2 was used in flutter calculations for Model 3.

FLUTTER CHARACTERISTICS

Models 1, 2, and 4 were tested to determine their flutter characteristics. Model 1 was tested until flutter was imminent and was then removed for the tunnel. Model 2 was tested until a static failure in bending occurred, with no evidence of flutter. The damaged model is shown in Figure 7. Model 4 was tested and removed before a static failure occurred, without evidence of flutter. Because of the similarity between Models 2 and 3, Model 3 was not tested after the static failure of Model 2.

Experimental values of the exponential decay factor and oscillation frequency for Model 1 are plotted in Figures 8 and 9, respectively. The highest speed attained was 24.2 knots. In view of the rapidly decreasing decay factors it was estimated that flutter would have occurred within one-half knot of the highest speed tested, so that a flutter speed of 24.7 knots is projected, with an uncertainty of ± 0.5 knot. The flutter frequency is projected to be 20.5 Hz, which was the lowest frequency that occurred during testing and which corresponded to the lowest decay factor. The reduced frequency at flutter is therefore 0.772, based on the above projected values.

The design flutter speed for Model 1 was 24.05 knots, with a flutter frequency of 17.5 Hz. Therefore the actual flutter speed was 3 percent higher than design, while the flutter frequency was 17 percent higher than the design value. The scaling of the parent model was successful in that flutter speed was reduced to a value close to half its original value, while

the discrepancy in flutter frequency can be explained by the deviation in the measured stiffnesses and, to a lesser degree, a small discrepancy in mass ratio.

The results for Model 1 demonstrate that it is possible to approach a hydrofoil flutter condition very closely without destroying the model. Very small speed increments were used to obtain a total damping value which was 54 percent of the structural damping or 1.3 percent of critical damping when testing of Model 1 was stopped. The decrease in total damping to a value smaller than the structural damping indicated that the hydrodynamic damping had already become negative. It is concluded that the flutter inception speed of a hydrofoil can be determined in some cases without the occurrence of flutter if damping measurements are made while speed is increased and if speed increments are kept small.

Model 2 was tested in the same manner as Model 1. However, Model 2 displayed excessively high static deflections during tip excitation in the speed range above 25 knots, and eventually failed in bending at 36 knots. Exponential decay factors and frequencies were measured using a maximum of 2 deg of tip twist up to 30 knots and are shown in Figures 10 and 11. The decay factors may have begun to decrease at 30 knots, but no further measurements were possible at this excitation amplitude because of the alarming deflections of the model. The deflections had a mean value which gradually decreased to the unstressed position after the excitation was released. During this decrease a few cycles of oscillation occurred. By reducing the excitation angle to 2/3 deg, the model was tested to 35 knots. The smaller excitation produced large decay factors which were beyond the scale of Figure 10 at 20 knots, and which could not be read at 25 knots and above. The large decay factors were caused by an excitation which did not sufficiently exceed the ambient flow fluctuations and by the tendency of the model to respond excessively at higher speeds. Model response to flow fluctuations at 35 knots was visible both on the oscillograph recordings and to the naked eye. Since damping could not be measured under these conditions, it was decided to increase tunnel speed gradually while recording model response until the model failed; the failure would have to be interpreted as either flutter or static failure due to divergence by the nature of the recorded signal. When the speed was increased to 36 knots, the model failed in bending, and several segments broke off, as shown in Figure 7. The strain gage output showed no oscillation, establishing that the failure was purely static.

It was expected that all of the models would fail similarly at about 36 knots, unless a flutter condition occurred at a lower speed as for Model 1. Since Model 3 was quite similar to Model 2, it would probably not flutter below 35 knots and would give no useful information by being tested. Model 4, however, had a substantially lower mass ratio than Model 2 and might possess a lower flutter speed. Therefore, Model 4 was tested up to 30 knots, with the resulting decay factors and frequencies shown in Figures 12 and 13. As in the case of Model 2, the measured decay factors were very high, and could not be read above 15 knots. Model excursions due to flow fluctuations were becoming visually noticeable at 30 knots, implying closeness to static failure. As has been previously described, air leakage from Model 4

necessitated several repairs to the Silastic seams. The value of further testing became more doubtful when all air leakage stopped during a run at 28 knots, indicating that the model had filled with water. A 60 Hz signal appeared in the strain gage output shortly afterward, further reducing its readability. Since the water had changed the inertial characteristics of the model, further testing was abandoned and the model was removed from the tunnel for retesting of its structural stiffnesses. Subsequent examination of the model showed a number of openings in the segments along the spar where pieces had broken off. Apparently flooding occurred through these openings in the segments rather than through the Silastic seams.

THEORETICAL FLUTTER ANALYSIS

The theoretical analysis was intended to explore the validity of the Yates flutter theory in the low mass range. It was recognized that the essential feature of the Yates theory was the modification that was made to two-dimensional Theodorsen loading in order to represent three-dimensional flow effects. Accordingly, the three calculations described below all incorporate spanwise variations in loading.

The structural representation used by Yates in his analysis was not considered to be an essential feature of the theory. Therefore, Yates' original six-mode Rayleigh-type analysis was not preserved in the present calculations. Instead, two calculations were made at NSRDC using a lumped parameter structural representation. A third calculation was made at SwRI using a two-mode Rayleigh-type analysis.

Both calculations made at NSRDC were corrected for structural damping as follows. An exponential decay factor δ_s based on the measured structural damping was added to the calculated decay factor δ_h . The factor δ_s was given by

$$\delta_s = \zeta_s \sqrt{\omega^2 + \delta_h^2}$$

and the total decay factor by

$$\delta = \delta_h + \delta_s$$

No structural damping was included in the calculation made at SWRI.

YATES FLUTTER THEORY

The first theory to be discussed employed the original Yates loading theory and will be referred to as the Yates flutter theory despite a different structural formulation than Yates used. The hydrodynamic loading of Yates consisted of stripwise application of two-dimensional Theodorsen loading, with loading due to circulatory flow modified for the effects

of finite span. The modification was accomplished by substituting three-dimensional distributions of lift slope and center of pressure location in place of the two-dimensional values of 2π and quarter chord, respectively. The three-dimensional spanwise distributions used were the same values used by Yates in his calculation for an aspect ratio 5 foil. These values, which were taken from Reference 11, are shown in Figure 14. The distributions were calculated with lifting surface theory.

The modified hydrodynamic loading was applied to a lumped parameter representation of the hydrofoil structure. The SADSAM III computer program^{15, 16, 17} was used to generate structural information based on measured model parameters. Each model was represented by structural stiffness and inertial parameters at 10 equally spaced spanwise stations at which hydrodynamic loading was applied. This permitted the calculation of 20 coupled structural modes.

Predicted natural frequencies in vacuum for Models 1 through 4 and the parent model are given in Tables 2 through 6. The predicted frequencies range from 5 percent high to 11 percent low, averaging 5 percent lower than experiment. The modes are labelled in Tables 2 through 6 according to predominant uncoupled mode components. The predicted nodal lines in Figure 6 show excellent agreement with experiment except for the second and third modes of Model 4. This discrepancy may have been caused by a structural irregularity in Model 4, as is suggested by the nodal line for the second mode. It was concluded that the structural representation was approximately correct for Models 1, 2, and 3, but not for Model 4. Despite the substantial variation in model densities, it is interesting to note that the mode shapes of all the models are nearly the same, except for the fifth and sixth modes of Model 4 which have interchanged their relative positions.

Using the zero-speed or noncirculatory part of Yates' hydrodynamic loading, the natural frequencies of the models in water were predicted and are given in Tables 2 through 6. The predicted frequencies range from 1 percent to 13 percent below experiment, and are on the average 9 percent low. This result implies that the noncirculatory hydrodynamic loading is not well represented in Yates' treatment.

Model response characteristics in the form of exponential decay factors were calculated as functions of speed for the four present models and the parent model. These are shown in Figures 8 through 13 and 15 through 18 along with the experimental results. Flutter is predicted to occur at a speed at which the exponential decay factor becomes zero. The predicted flutter speeds and frequencies are indicated in each figure.

According to the two flutter speeds that were obtained experimentally, the predictions of the Yates theory were overconservative. The 20.1-knot prediction for Model 1 was 23 percent below the observed flutter speed, and the 33.7-knot prediction for the parent model was 30 percent below experiment. Similarly, the 26.4-knot flutter prediction for Model 2 was 27 percent below the static failure speed of the model. The magnitudes of the predicted decay factors were much lower than the observed magnitudes throughout the speed range, showing

that damping was consistently underestimated. Frequency predictions were consistently below experiment at low speeds and above experiment at high speeds. No indication was evident in the calculations of the decrease in flutter speed which had been found at low values of mass ratio in the Yates study.

NSRDC FLUTTER THEORY

The second theory to be discussed consisted of an extension of the Yates theory previously described. The extended theory modified the noncirculatory loading to account for three-dimensional flow effects. This extension was based on a suggestion made by Yates in Reference 7.

The noncirculatory loading terms were multiplied by a spanwise function which was inferred from the virtual mass expression for a flat plate. This modification was chosen in view of the presence of virtual mass and moment in the noncirculatory loading expression. The function consisted of the fraction of two-dimensional virtual mass of the foil outboard of the spanwise position being considered and was given by

$$p = \frac{A^*}{\sqrt{1 + (A^*)^2}}$$

In this expression A^* is the local aspect ratio, which is the aspect ratio of the foil outboard of the local position, when a reflecting plane exists at the local position. The distribution factor p is shown in Figure 19 for an aspect ratio 5 hydrofoil. Total virtual mass values from this function agreed well with measured values given in Reference 1.

Predicted natural frequencies in still water for the five models are given in Tables 2 through 6. The predictions range from 10 percent above experiment to 9 percent below, averaging 1 percent above the measured values. These results are significantly better than the predictions of the unmodified Yates theory, and it is concluded that noncirculatory loading is well represented by the spanwise function used.

Model flutter characteristics calculated by the NSRDC flutter theory are shown in Figures 8 through 13 and 15 through 18. The flutter speed predictions of the NSRDC flutter theory were conservative, but not overconservative as were those of the Yates flutter theory. The predicted flutter speed of 23.1 knots for Model 1 was 7 percent lower than experiment, while the Yates theory predicted a flutter speed which was 23 percent low. Similarly, the 41.8-knot prediction for the parent model was 13 percent below experiment, as compared to a Yates theory prediction which was 30 percent low. Flutter speeds for the remaining models were predicted to be higher according to the NSRDC theory than according to the Yates theory, although the prediction for Model 2 was still below the failure speed of 36 knots. Frequency predictions of the NSRDC theory were fairly accurate over the speed range tested and showed slightly better agreement with experiment than the Yates theory predictions.

In addition to the more accurate flutter speed predictions of the NSRDC theory, the decay factors were more accurately predicted over the entire speed range in comparison with the Yates theory. The improvement consisted of an increase in the predicted decay factors to approximately the measured values.

The predicted decay factors and flutter speeds of both the NSRDC theory and the Yates theory were significantly affected by inclusion of structural damping. This raised the calculated flutter speeds from 10 to 35 percent for the Yates theory and from 6 to 14 percent for the NSRDC theory. It is therefore concluded that structural damping was not negligible for the present models and should be included in future experimental and theoretical studies.

SWRI FLUTTER THEORY

The third theory to be discussed is another modification of the original Yates flutter theory, and is described as Case 6c in Reference 11. It will be referred to as the SwRI flutter theory. In this calculation, two-dimensional Theodorsen hydrodynamic loading was modified to incorporate measured spanwise lift slopes. The lift slope distribution used is shown in Figure 14a. The center of pressure location was left unchanged from its quarter chord position corresponding to two-dimensional flow. The hydrodynamic loading was integrated over the span of the model in a two-mode Rayleigh-type analysis. No structural damping was included.

Flutter characteristics of the hydrofoil models calculated by the SwRI theory are shown in Figures 8-13 and 15-18. The flutter speed predictions agreed very closely with the two experimental flutter speeds, and were more accurate than the NSRDC predictions. Furthermore, the prediction of 48.0 knots for Model 2 was above the speed at which the model failed, so that the SwRI theory may not be as conservative at low mass ratios as the two theories previously discussed. The agreement between measured and calculated decay factors was very good. Frequency predictions were slightly lower than the NSRDC theory predictions. The response curves for the first mode were not graphed, but were found to be stable.

DISCUSSION

The flutter speed predictions of all three theories have been plotted in Figure 20 as functions of mass ratio. All theories predicted an increasing flutter speed as mass ratio decreased, for the mass ratios of the models tested. The flutter curves retained their relative positions throughout the mass ratio range, with the Yates theory predicting the lowest flutter speeds, the NSRDC theory predicting slightly higher flutter speeds, and the SwRI theory predicting the highest flutter speeds.

The failure of the three flutter theories to predict a flutter speed boundary which decreased as mass ratio decreased in the low mass ratio range was unexpected in view of the Yates prediction in his original analysis.⁷ The decreasing flutter speed found by Yates

occurred below a mass ratio of approximately 0.3. Differences between the present theories and the original Yates theory may have accounted for the discrepancy. A similar downturn may occur for the present theories below a mass ratio of 0.202, but no calculations were made to determine whether this does occur.

Test results established that all theories were conservative at mass ratios 0.99 and 0.963. The Yates theory and the NSRDC theory were also conservative at mass ratio 0.455. The other predictions could not be evaluated because the predicted flutter speeds were higher than the observed bending failure speed.

The noncirculatory loading modification used in the NSRDC flutter theory is a significant improvement over the unmodified Yates hydrodynamic loading. The modification produced more accurate natural frequency predictions for the hydrofoils in still water as well as improved flutter predictions. The effect of this modification on flutter predictions at very low mass ratio was not determined.

Although the SwRI flutter theory gave the most accurate flutter predictions, it has less capability than the NSRDC flutter theory for solving flutter problems of full-scale hydrofoil systems. The deficiency of the SwRI theory lies in its use of only two structural modes of vibration. Two modes cannot adequately represent the structural properties of a complex strut-foil system. The theory could be expanded to include a larger number of modes, as was done in the original 6-mode analysis of Yates. However, the lumped parameter structural representation used in the NSRDC theory is extremely versatile in representing complex structures, including pods and foils attached to struts. It would be possible to combine the lumped parameter representation with the hydrodynamic loading used in the SwRI theory, but this should await further experimental confirmation of the SwRI theory.

THEORETICAL DIVERGENCE ANALYSIS

The structural failure of Model 2 at 36 knots indicated a need for further analysis of the divergence characteristics of the flutter models. Model design had been based on two-dimensional load theory, which had predicted a center of pressure at the quarter chord of the model and consequently, an infinite divergence speed. Although a divergence failure had not been predicted, structural failure was predicted to occur as a result of bending stress as a function of foil angle and speed. For example, a uniform foil angle of 3.6 deg or a tip twist angle of 6.8 deg would have caused the spar to yield at 36 knots.⁹ Since model trim and tip excitations had been held to much smaller values than these, the observed failure cannot be explained by this prediction. It is concluded that the two-dimensional load theory is inadequate to predict the loading on the foil.

A more accurate prediction of failure characteristics could use three-dimensional lifting surface theory, which predicts a center of pressure location forward of the quarter chord on finite aspect ratio foils. A forward location of the center of pressure would increase the

probability of either divergence or bending failure by causing torsional deflections to increase, thereby increasing the stress on the model.

Therefore, the Yates hydrodynamic loading formulation, previously used in the Yates flutter theory and based on a three-dimensional lifting-surface calculation of lift slope and center of pressure, was used to calculate model failure characteristics. The steady loading terms were combined with the lumped parameter stiffness matrix used in the flutter calculation. In matrix form, resulting equations for the 10 spanwise stations used are

$$\begin{aligned} [K_h] &= \{P_0(\alpha_i)\} \\ & \quad i = 1, 2, \dots, 10 \quad (1) \\ [K_\theta] &= \{M_0(\alpha_i)\} \end{aligned}$$

where $[K_h]$ = bending stiffness matrix,

$[K_\theta]$ = torsional stiffness matrix,

$P_0(\alpha_i)$ = steady lift on foil due to angle of attack,

$M_0(\alpha_i)$ = steady moment on foil due to angle of attack,

h_i = local translational displacement of foil elastic axis from unstressed position,

θ_i = local torsional displacement of foil elastic axis from unstressed position, and

α_i = local angle of attack between foil and free stream.

The coordinates h and θ correspond to elastic displacements of the foil spar. They are referred to the unstressed position of the foil, not to the flow direction, and are zero when, for example, the foil is motionless in still water. On the other hand, the angles α_i are defined as the angles that local chords make with the free stream. Thus the α_i include both structural twist angles and misalignment angles between the foil and the flow direction. The composite nature of the α_i can be expressed by the relation

$$\alpha_i = \theta_i + \gamma_i$$

where γ_i = local angle of unstressed foil relative to the free stream. Relationships among the three angular coordinates are shown in Figure 21.

Since the lift and moment expressions are proportional to angle of attack α_i , Equation (1) may be written

$$\begin{aligned} [K_h] \{h_i\} &= \{P_0(\theta_i)\} + \{P_0(\gamma_i)\} \\ [K_\theta] \{\theta_i\} &= \{M_0(\theta_i)\} + \{M_0(\gamma_i)\} \end{aligned}$$

The terms in the second of the above equations can be combined to give

$$[K_\theta - \bar{M}] \{\theta_i\} = \{M_0(\gamma_i)\} \quad (2)$$

where $\{\bar{M}\}$ is a diagonal matrix defined by

$$\{\bar{M}\} \{\theta_i\} = \{M_0(\theta_i)\}$$

A non-trivial solution to the homogeneous form of Equation (2) exists when the determinant of the coefficient matrix vanishes. The determinant will vanish for some value or values of free stream velocity U_D . U_D is the divergence speed because the vanishing of the determinant of $[K_\theta - \bar{M}]$ implies that all θ_i are infinite for a non-zero set of values $\{M(\gamma_i)\}$. For speeds below U_D , Equation (1) can be solved for specified initial flow misalignment angles γ_i to give the bending and torsional displacements of the foil. Stress values can then be determined from the displacements.

The divergence speed of Model 2 was calculated using the stiffness matrix $[K_\theta]$ and the steady part of the hydrodynamic loading which had been previously used in the Yates and NSRDC flutter calculations. A value of 44.0 knots was obtained for U_D . Since this speed was substantially higher than the observed failure speed, further calculations were made to determine whether the model might have failed in bending prior to reaching divergence.

The response of a typical hydrofoil to hydrodynamic loading near the divergence speed has been discussed in Reference 18. The response of the foil varies from zero at zero speed to infinity at the divergence speed. Foil torsional deflection may be described in terms of a magnification effect in which ratio of the model tip twist angle to the misalignment angle varies from zero to infinity. When the ratio is unity, a given misalignment angle produces an equal tip twist. This magnification ratio was calculated using the lumped parameter representation for Model 2 and is shown in Figure 22. The misalignment angle was assumed to be constant along the span of the model for purposes of calculation. Unit magnification of misalignment angle occurs at 26.5 knots, or 60 percent of the divergence speed. At 36 knots it is predicted that the structural twist of the model tip will be 3.5 times the misalignment angle.

Correspondingly high bending displacements are predicted to accompany the torsional displacements. In order to determine the approximate misalignment angle that would cause failure in bending, a spar yield boundary was calculated using the yield stress of the spar, 350,000 lb/sq in. This boundary is plotted in Figure 23. A misalignment angle of 0.92 deg was predicted to cause bending failure at 36 knots.

Motion pictures of Model 2 showed that ambient flow fluctuations caused tip deflections of as much as 1 deg in torsion and 0.4 in. in bending, about the mean position, at 35 knots. The flow fluctuation angles were not measured directly.

On the basis of calculated model response and observed model deflections it is concluded that Model 2 failed structurally in bending at 36 knots. The failure was caused by too close an approach to the divergence speed of the model. The failure was initiated by small flow fluctuations in the tunnel jet which were magnified by the model divergence characteristics. Each of the other models would have failed similarly at nearly the same speed because of their similar elastic properties.

The divergence theory used agrees reasonably well with observed model behavior. Future model design should be based on a similar divergence calculation. In order to test a model successfully at a given speed the divergence speed must be substantially higher than the test speed. An appropriate test speed limit might be 60 percent of the calculated divergence speed, at which speed the response of Model 2 equalled the flow fluctuation angle. At this speed model response to either flow fluctuations or deliberate excitation would be limited to the initial disturbance amplitude and would cause little interference with damping measurements. Additional calculations would be required to ensure that the model would not fail in bending as a result of the model excitation.

The divergence speed of models of the present type could be increased by placing the elastic axis farther forward, in order to have the center of pressure of the loading aft of the elastic axis. Figure 24 illustrates the dependence of theoretical divergence speed on elastic axis position for Model 2. If the elastic axis were located at $a = -0.58$, corresponding to an elastic axis at 21 percent of the chord aft of the leading edge, the predicted divergence speed would be 83.3 knots and a test speed of 50 knots would equal 60 percent of the divergence speed.

CONCLUSIONS

Four hydrofoil models were constructed which successfully scaled a previously-tested hydrofoil to smaller size and to lower mass ratios. Flutter was obtained for the model of mass ratio 0.963. The models of mass ratio 0.455, 0.395, and 0.202 were subject to static failure in bending before flutter was encountered.

The results for Model 1 demonstrate that it is possible to approach a hydrofoil flutter condition very closely without destroying the model. It is concluded that the flutter inception speed of a hydrofoil can be determined in some cases without the occurrence of flutter if damping measurements are made while speed is increased, and if speed increments are kept small.

The flutter characteristics of the models were calculated using three versions of the Yates hydrodynamic loading theory. Both the Yates flutter theory and the NSRDC flutter theory showed a tendency to be overconservative. Inclusion of structural damping in these calculations had a significant effect on calculated flutter speeds. The SwRI flutter theory agreed well with experiment at mass ratios of 0.963 and 0.99, but could not be confirmed at lower values of mass ratio.

A spanwise modification to the noncirculatory loading, contained in the NSRDC theory, significantly improved the predictions of natural frequencies in water and of model damping characteristics and flutter speeds. Additional calculations are required to determine the nature of the low mass ratio flutter boundary with and without this modification.

The static bending failure observed on the mass ratio 0.455 model was caused by too close an approach to the divergence speed of the model. The failure was initiated by small flow fluctuations in the tunnel jet which were magnified by the model's divergence characteristics. Each of the other models would have failed similarly at nearly the same speed because of the similar elastic properties of the models. The observed failure was consistent with the calculated divergence speed of 44 knots.

RECOMMENDATIONS

1. The present tests were unsuccessful in defining flutter boundaries at low mass ratio because of structural failure of the models. Future small-scale flutter-model design should employ three-dimensional hydrodynamic load theory in calculating the spanwise center of pressure location for divergence speed predictions. Test speeds should be limited to 60 percent of the divergence speed to eliminate undue model deflections and to preclude structural failure.

2. Full-scale hydrofoil craft utilize low mass ratio struts with relatively massive pods and foils attached to the ends of the struts. It has been shown that flutter speeds of struts can be radically lowered by such tip elements.^{1, 19} The effects of foil configuration, pod inertia and shape, and submergence depth should be further investigated both experimentally and theoretically. Addition of tip masses would permit flutter testing of models similar to those described in this report.

3. Future flutter testing should utilize damping measurement to detect the approach of flutter. Methods of damping measurement should be developed for eventual use on full-scale hydrofoil craft.

PERSONNEL AND ACKNOWLEDGMENTS

The present work was accomplished by cooperation of the staffs of the Naval Ship Research and Development Center and Southwest Research Institute. Design and construction of the test apparatus was carried out at SwRI under the direction of Guido E. Ransleben, Jr. Vibration and flutter tests were performed at NSRDC by Besch and Ransleben, the data analysis and report by Besch. Flutter calculations were performed by Dr. Wen-Hwa Chu at SwRI. Structural mode and flutter calculations were performed by Dr. Liu at NSRDC.

Invaluable assistance in all phases of the present work was given by Daniel S. Cieslowski of NSRDC and Dr. H. Norman Abramson of SwRI. Mr. Cieslowski's assistance during vibration and flutter testing was particularly appreciated.

The contributions of the following NSRDC personnel are also gratefully acknowledged:

Harry D. Harper who provided the test instrumentation and assisted during the flutter testing; Richard K. Brown and Robert O. Farmer who performed the forced oscillation testing of the models; and Robert A. Briggs who designed the pressure regulation system for the model support enclosure. Willis L. Mynatt of SwRI also provided valuable assistance during vibration and flutter testing.



Figure 1 - Spar and Ballasted Segments before Assembly

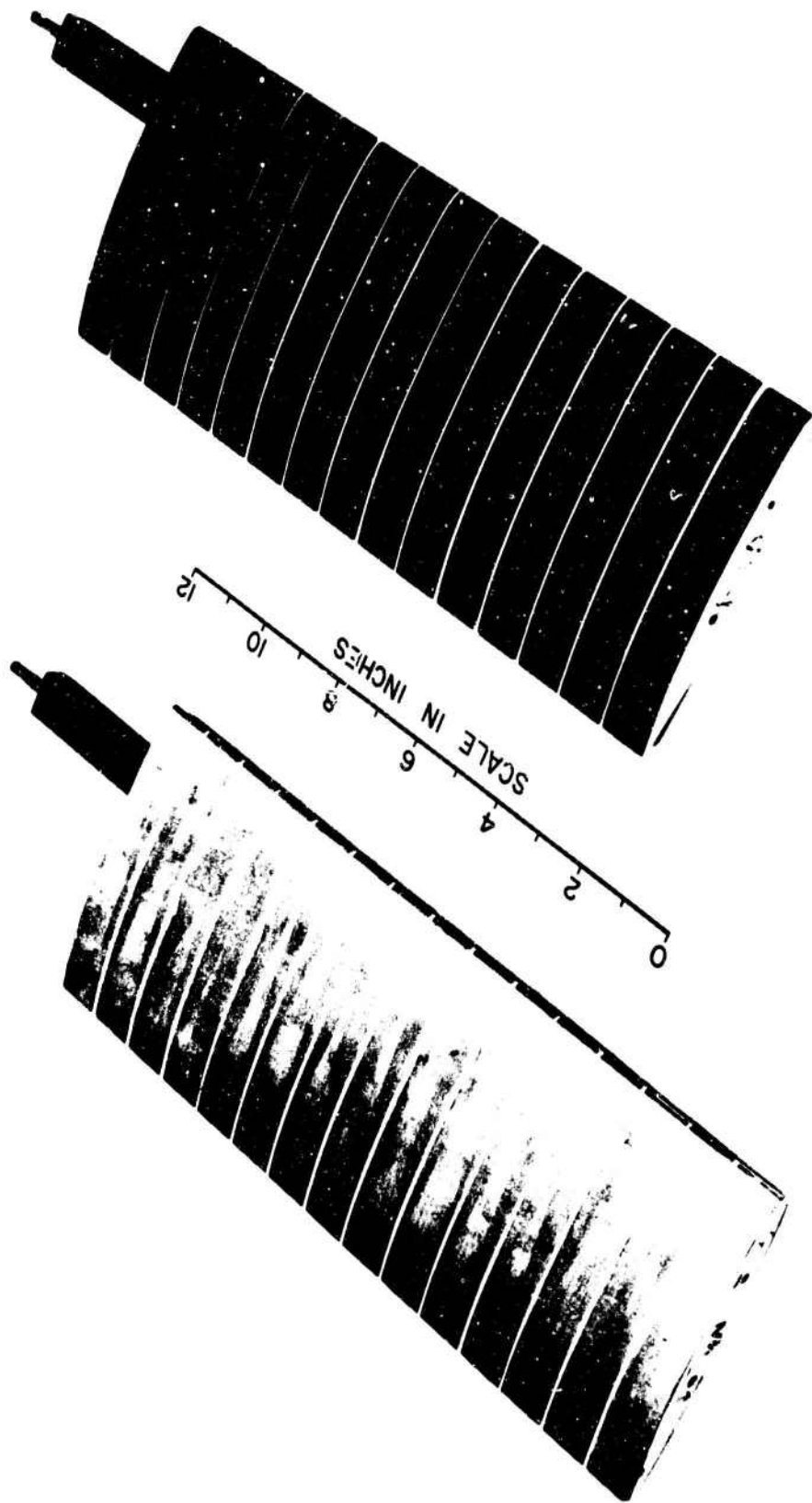


Figure 2 -- Completed Models

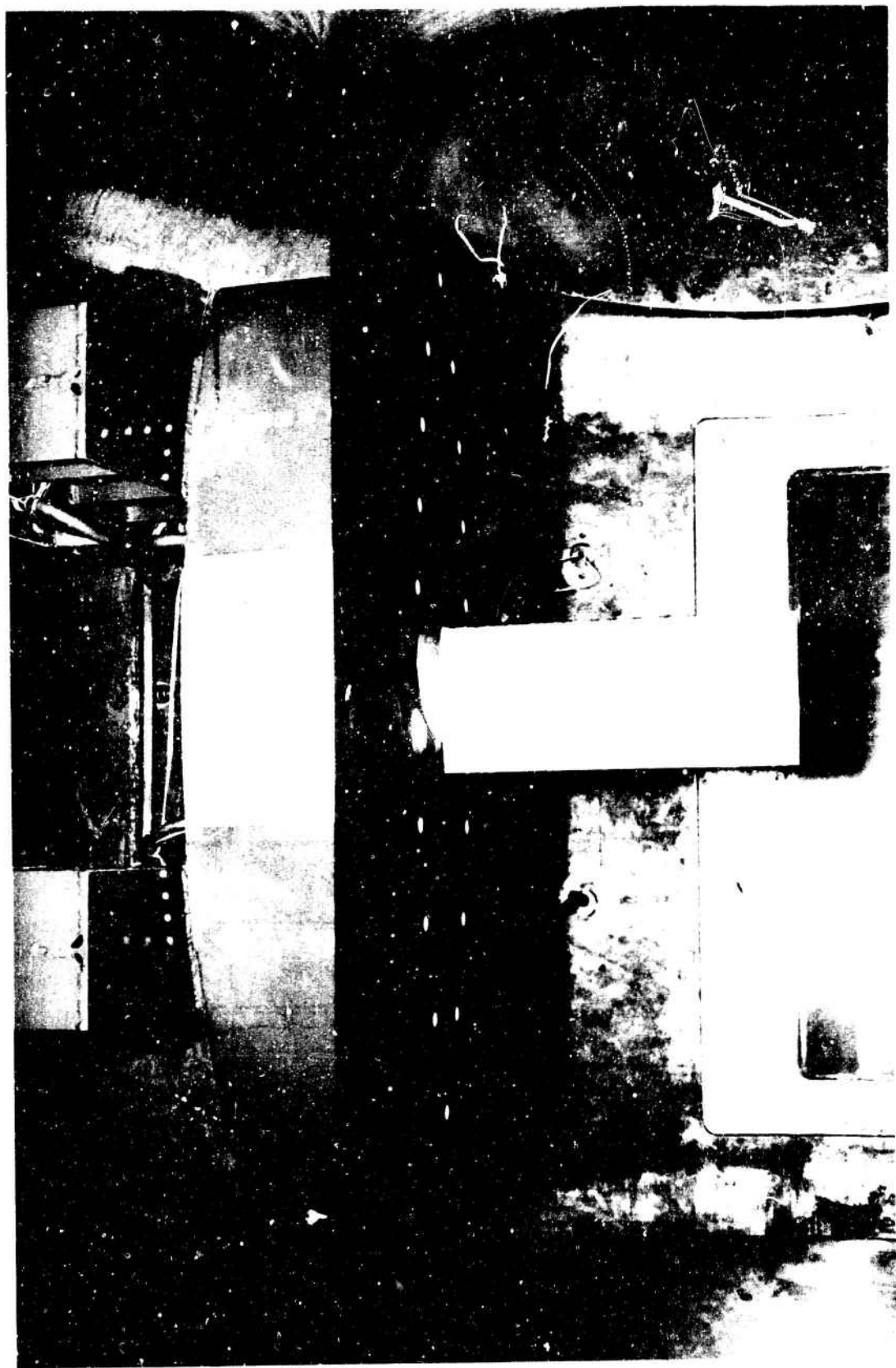


Figure 3 — Flutter Model and Model Support Enclosure Mounted in 36-Inch Variable Pressure Water Tunnel

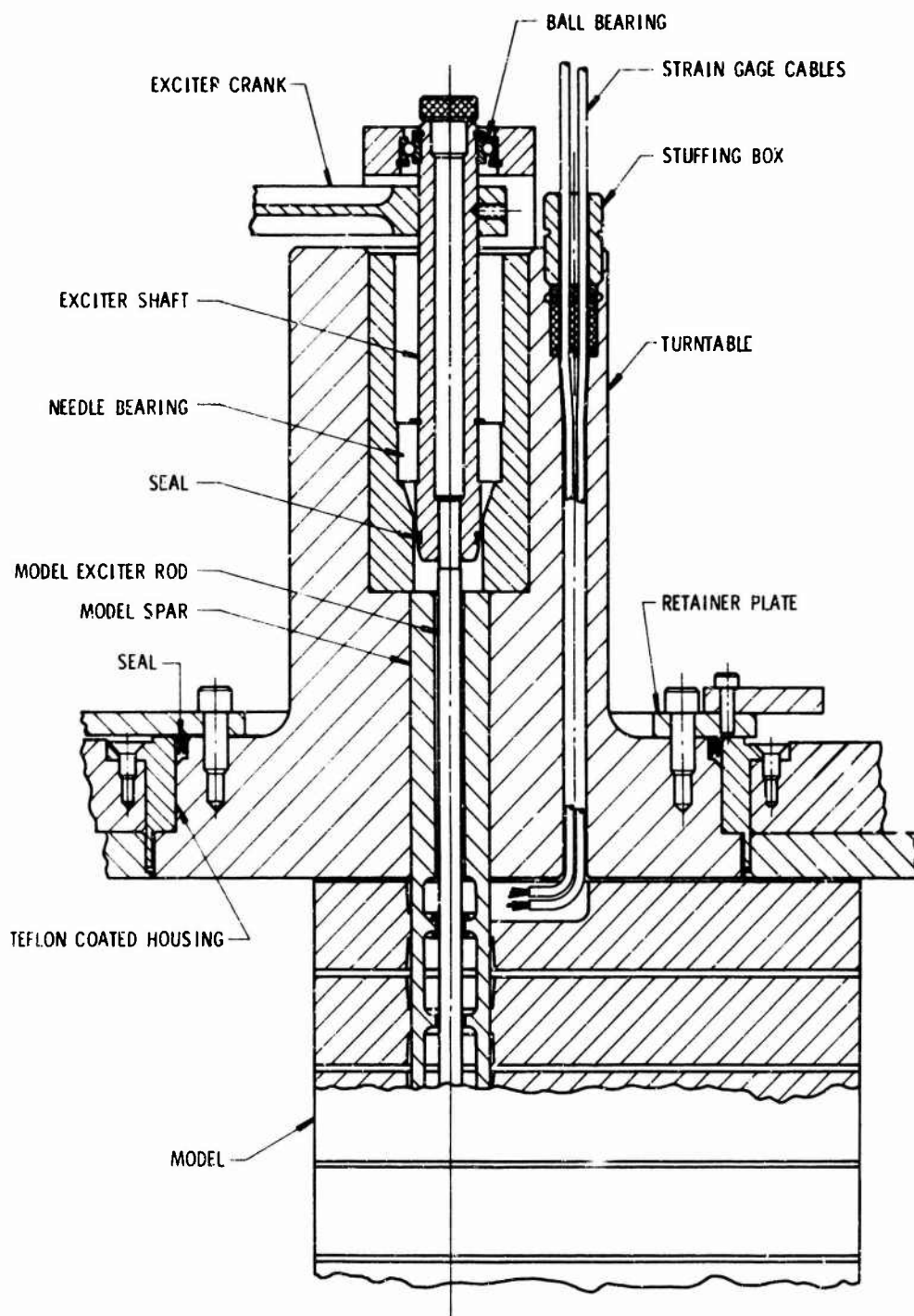


Figure 4 - Section through Turntable

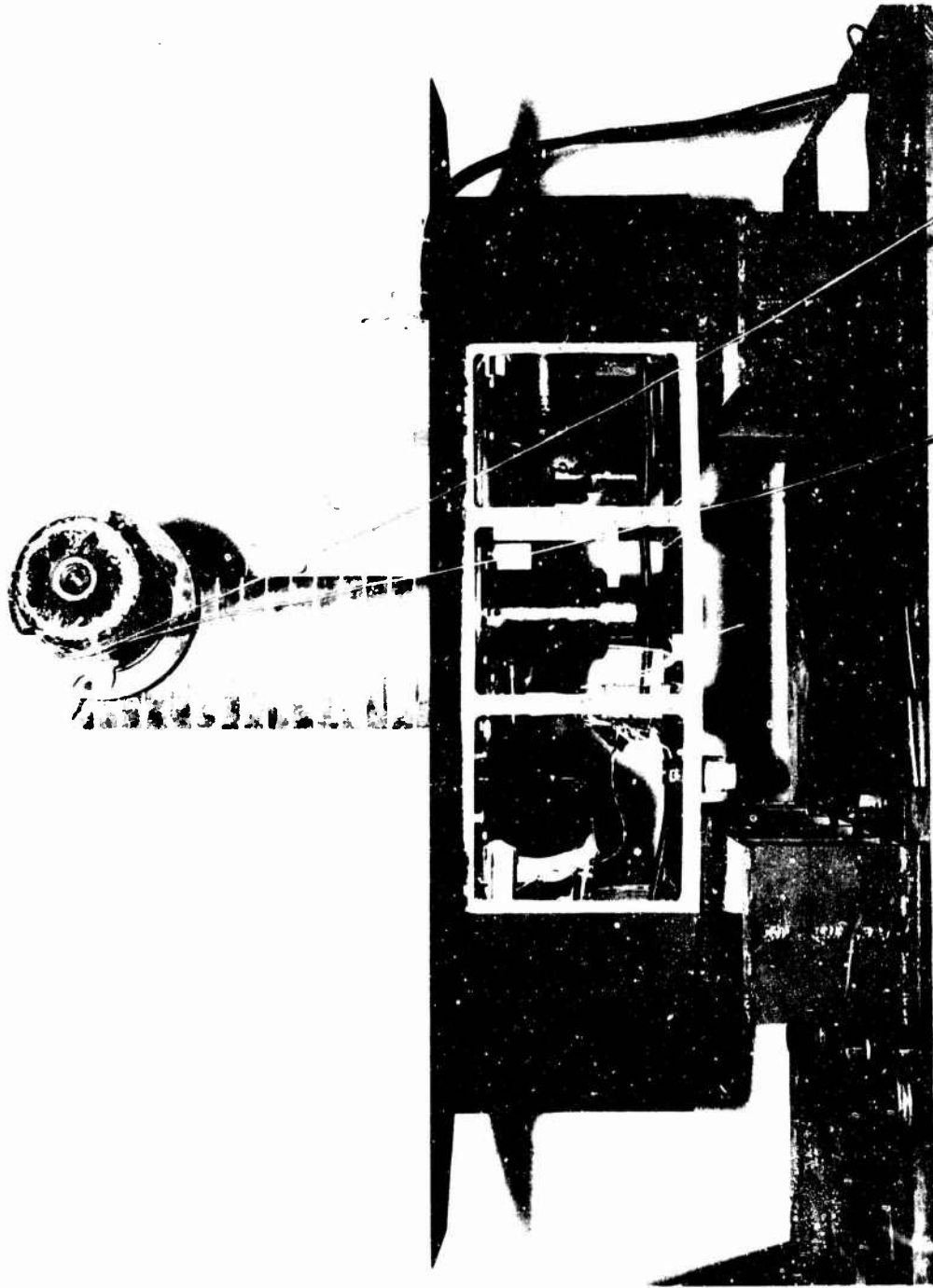


Figure 5 — Excitation of Flutter Model by Electromagnetic Oscillation

Figure 6 – Theoretical and Experimental Nodal Lines for the First Six Natural Frequencies of Flutter Models in Air

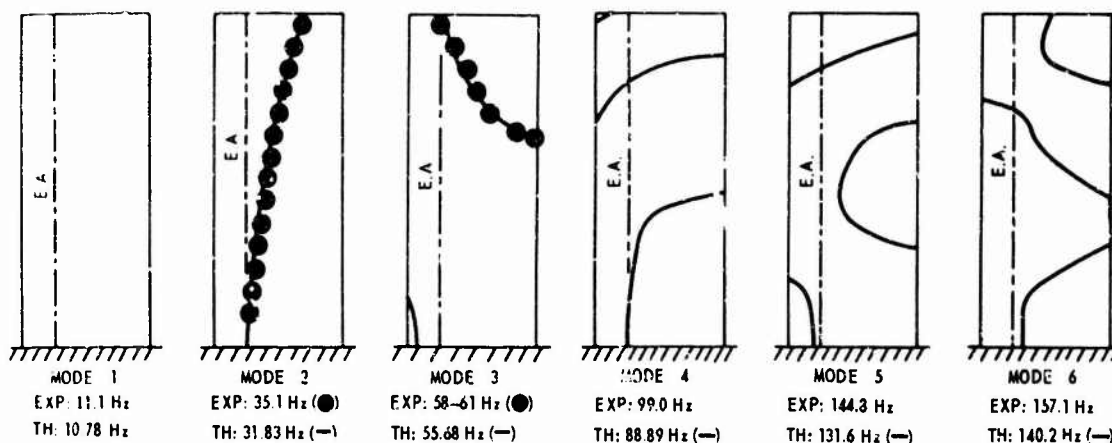


Figure 6a – Model 1

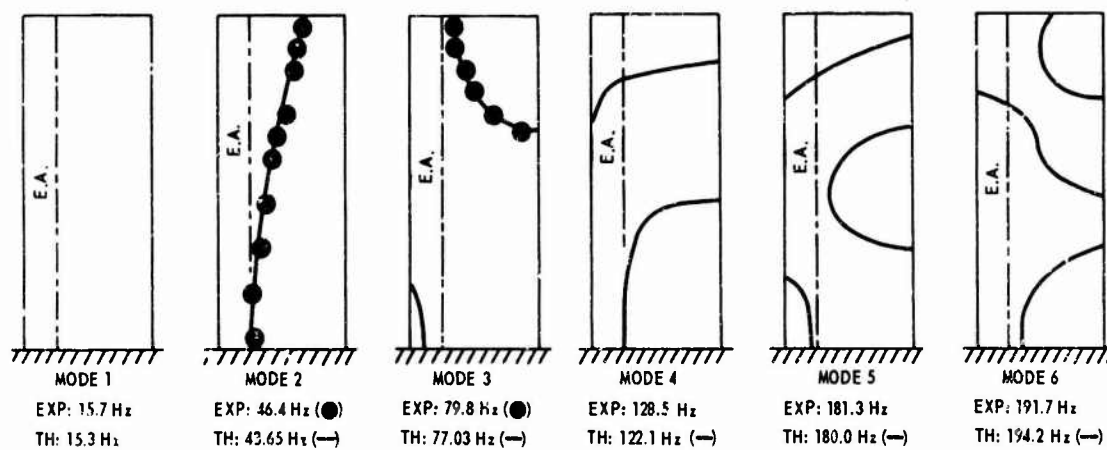


Figure 6b – Model 2

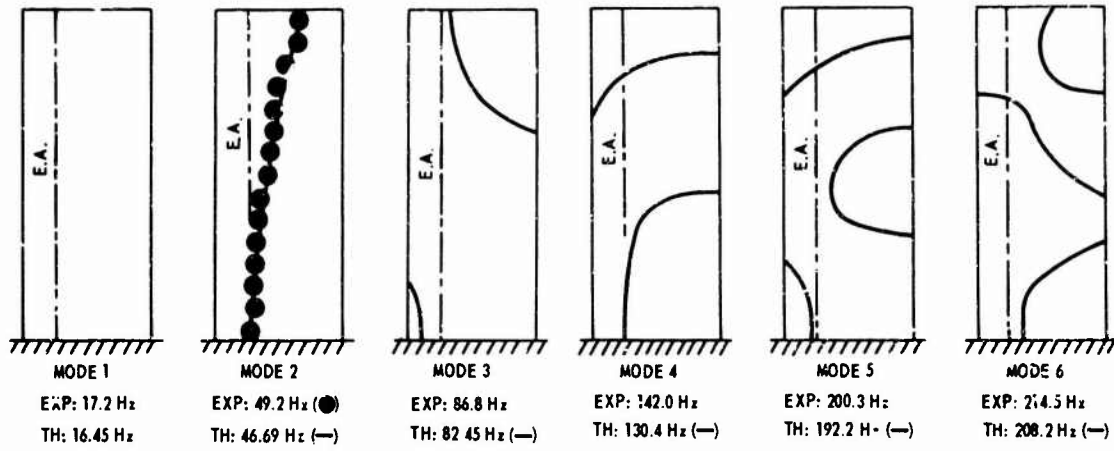


Figure 6c - Model 3

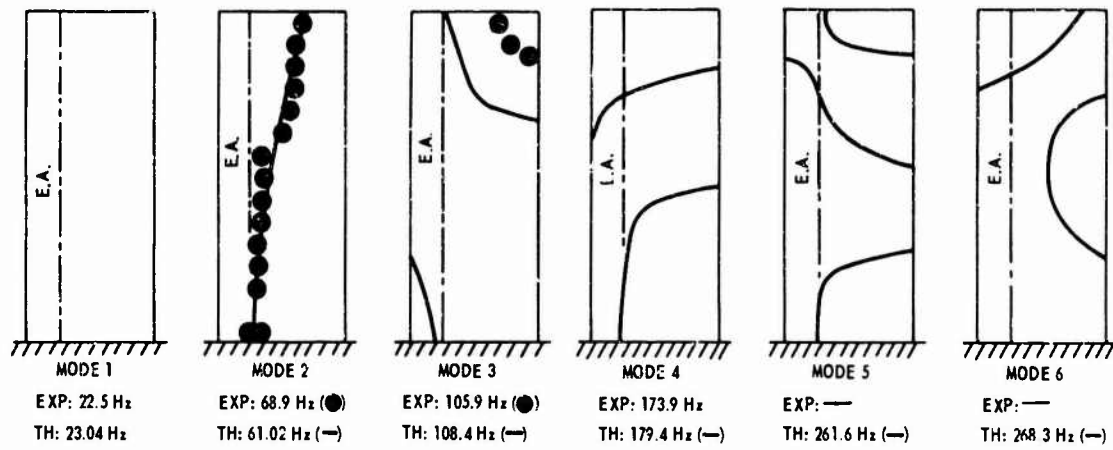


Figure 6d - Model 4

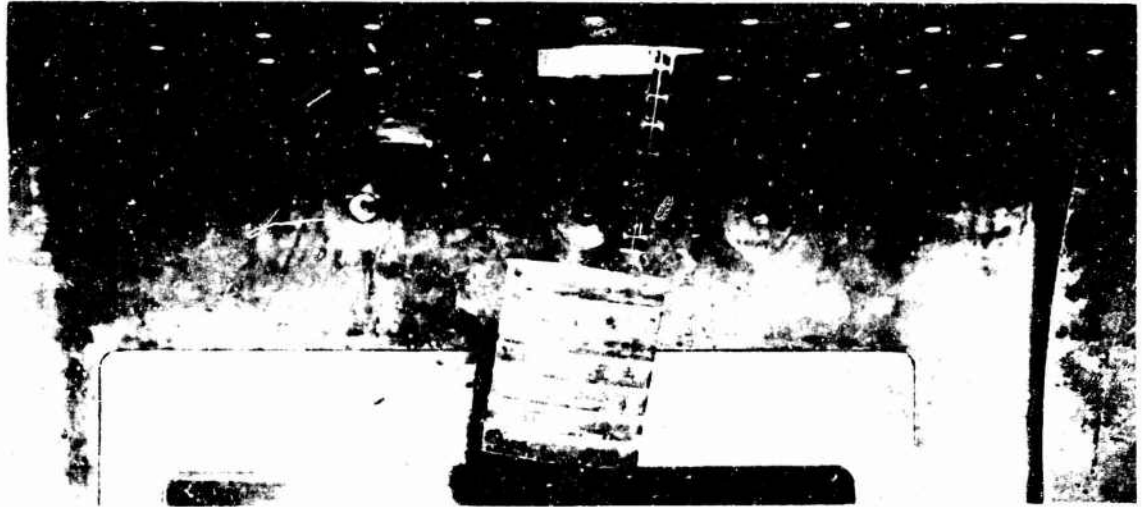


Figure 7b - After Removal from Tunnel

Figure 7 - Model 2 after Static Failure in Bending

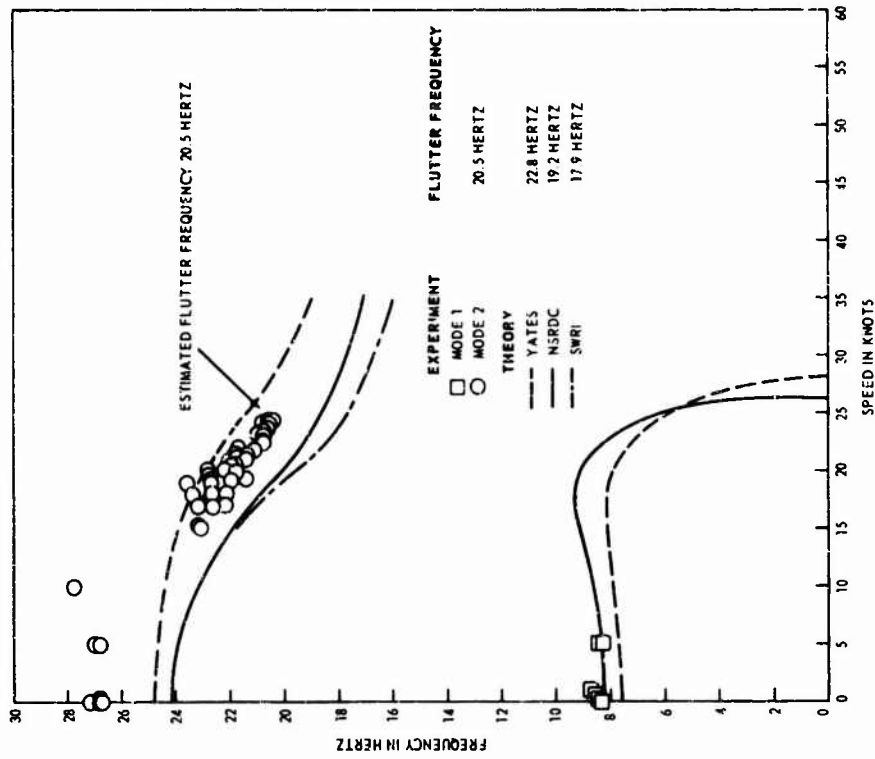


Figure 9 - Frequency as a Function of Speed for Model 1

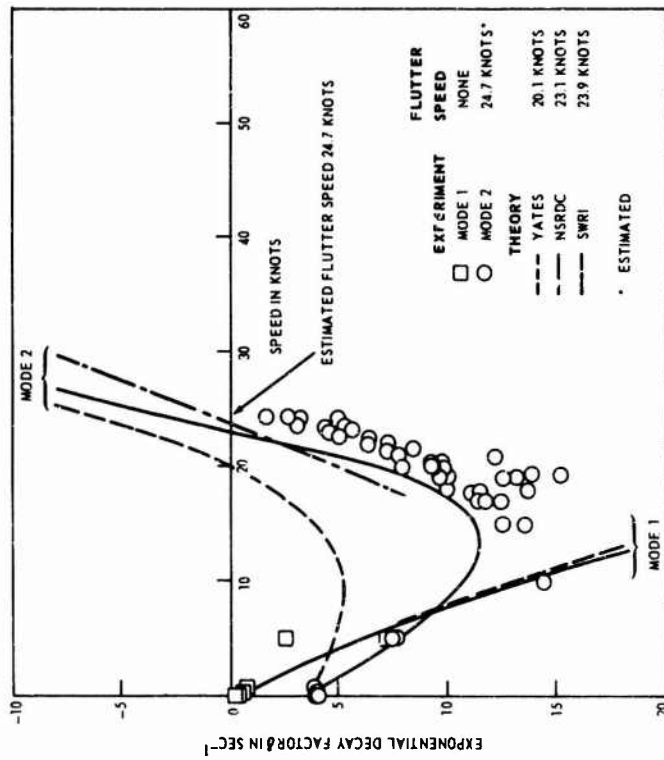


Figure 8 - Exponential Decay Factor δ as a Function of Speed for Model 1

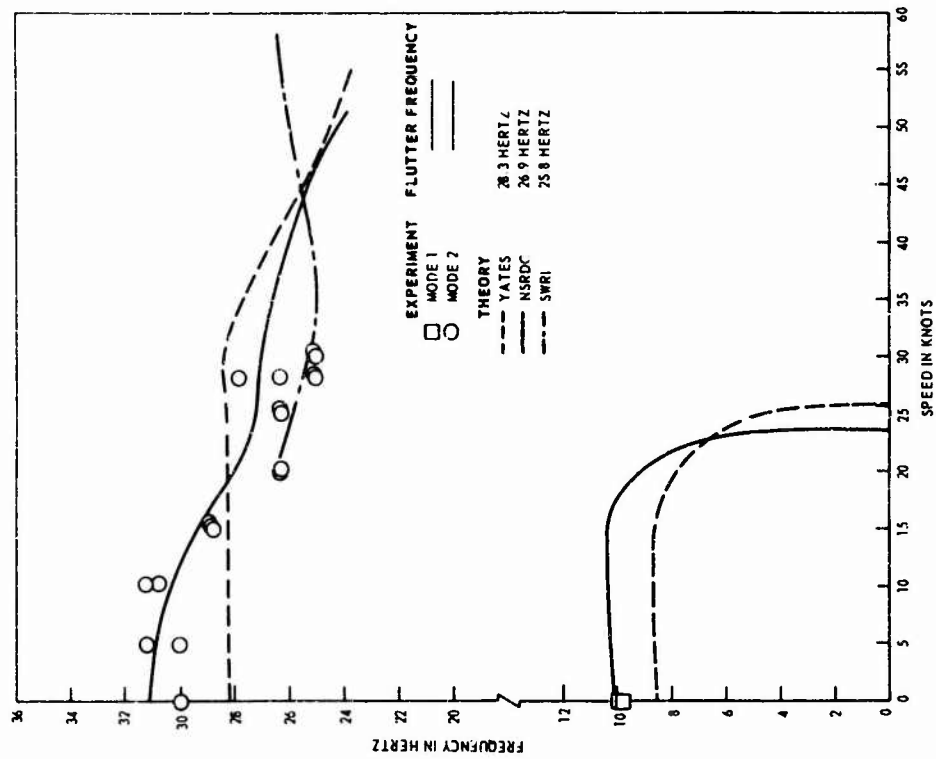


Figure 11 - Frequency as a Function of Speed for Model 2

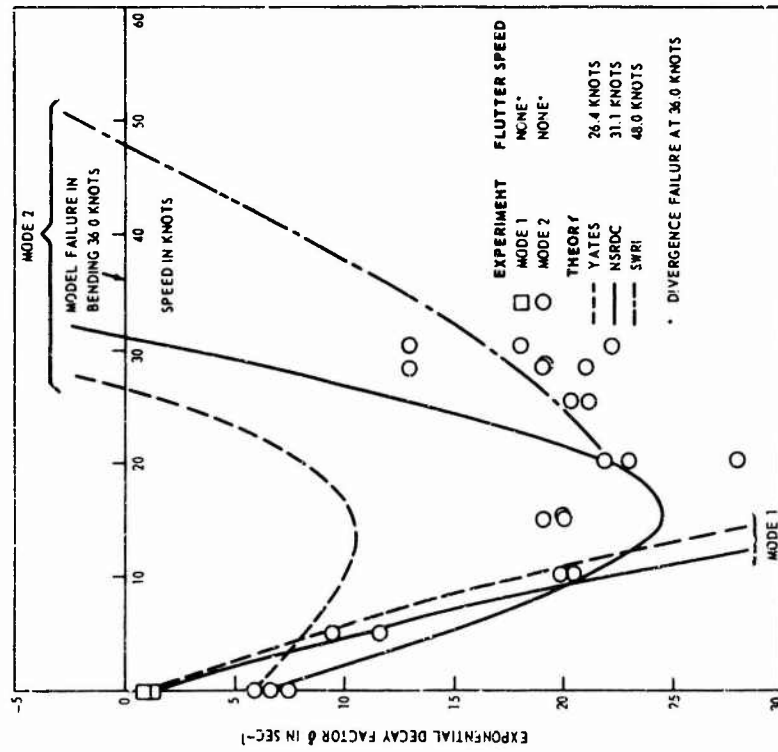


Figure 10 - Exponential Decay Factor δ as a Function of Speed for Model 2

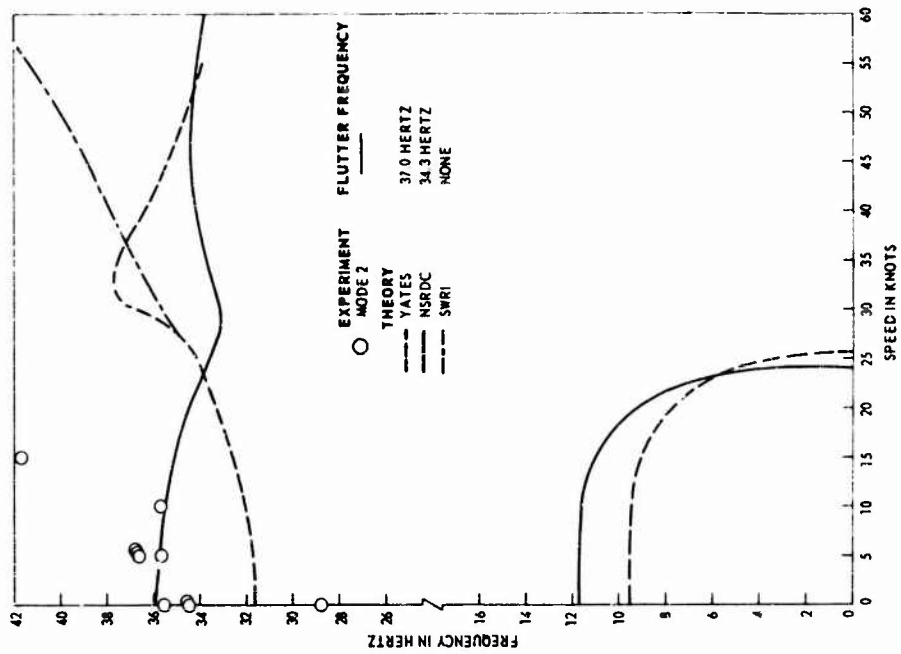


Figure 13 - Frequency as a Function of Speed for Model 4

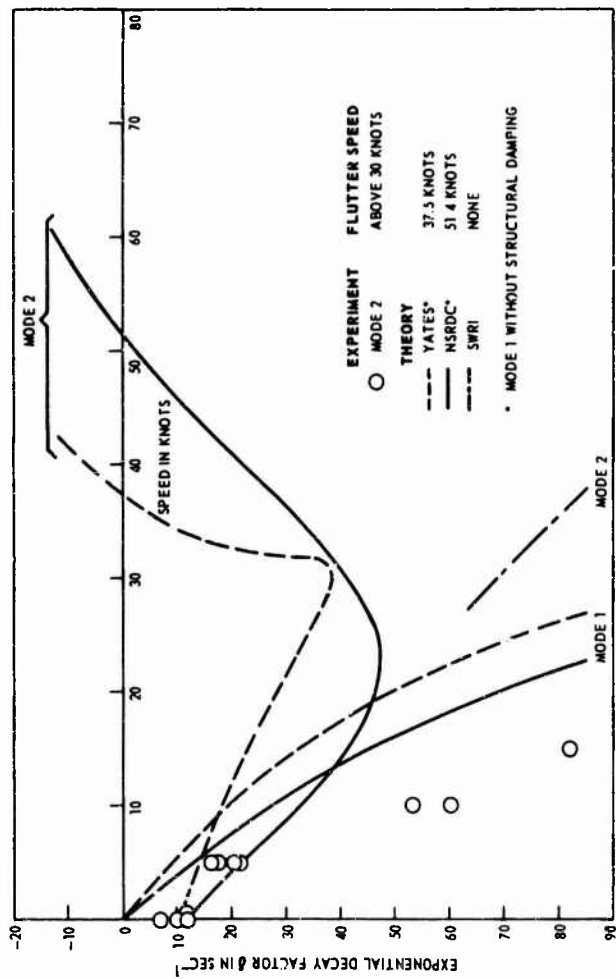


Figure 12 - Exponential Decay Factor δ as a Function of Speed for Model 4

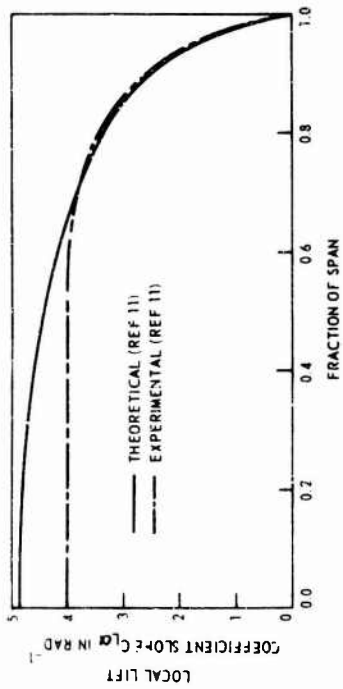


Figure 14a - Local Lift Coefficient Slope

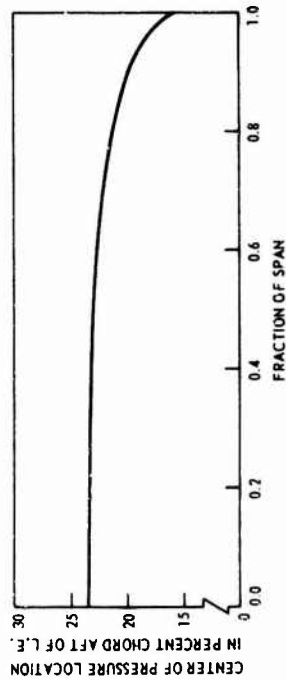


Figure 14b - Spanwise Distribution of Center of Pressure

Figure 14 - Spanwise Load Distributions for Aspect Ratio 5 Rectangular Foil

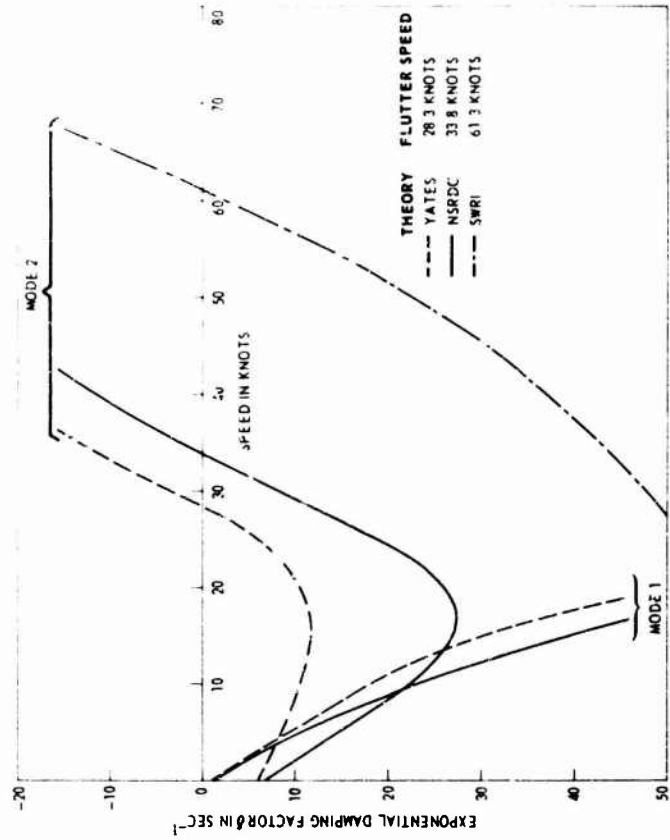


Figure 15 - Exponential Decay Factor δ as a Function of Speed for Model 3

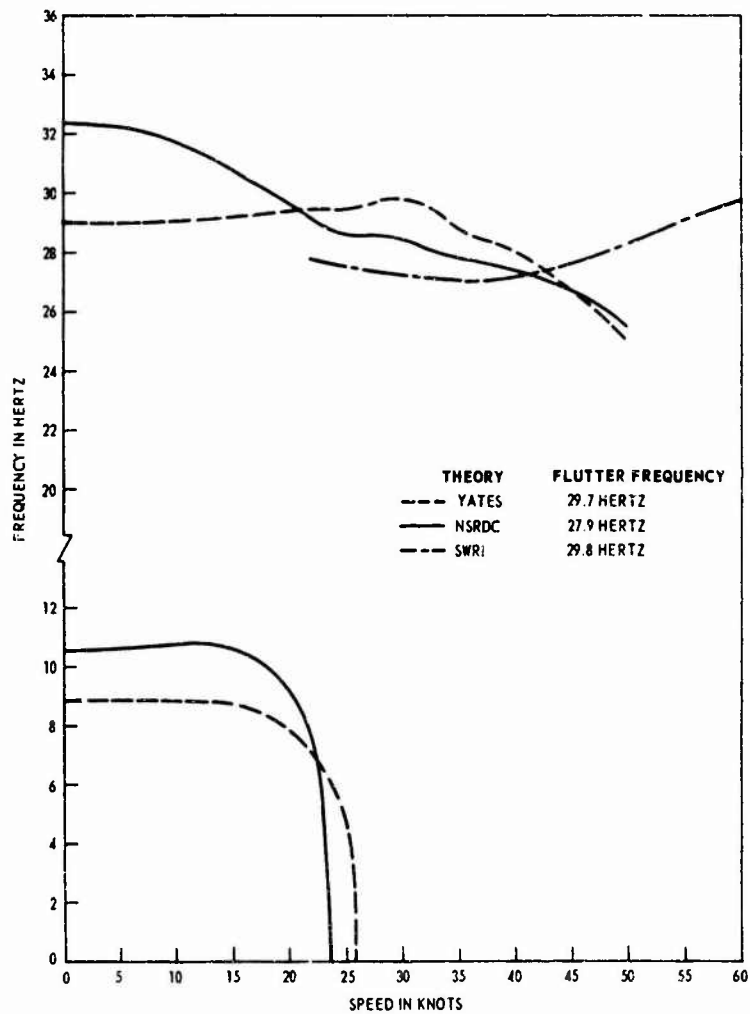


Figure 16 – Frequency as a Function of Speed for Model 3

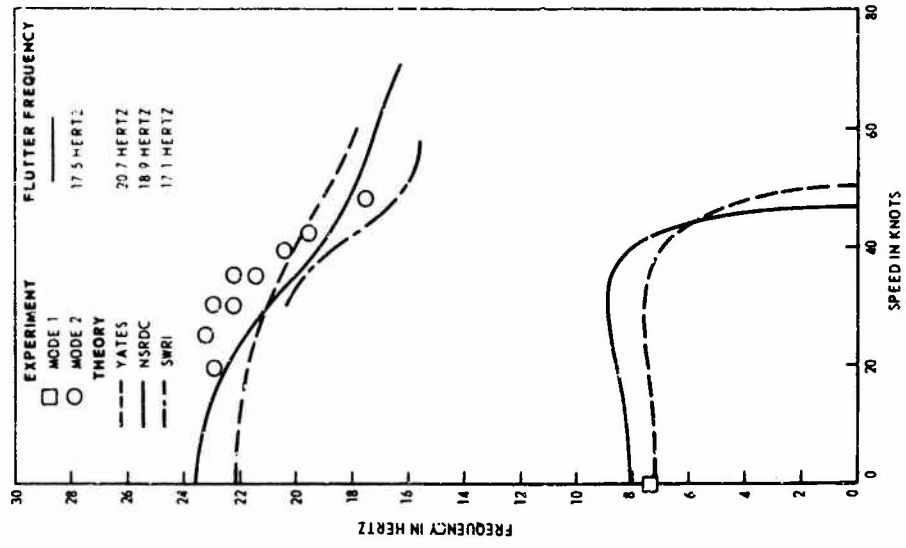


Figure 18 — Frequency as a Function of Speed for the SwRI 30-Inch Flutter Model

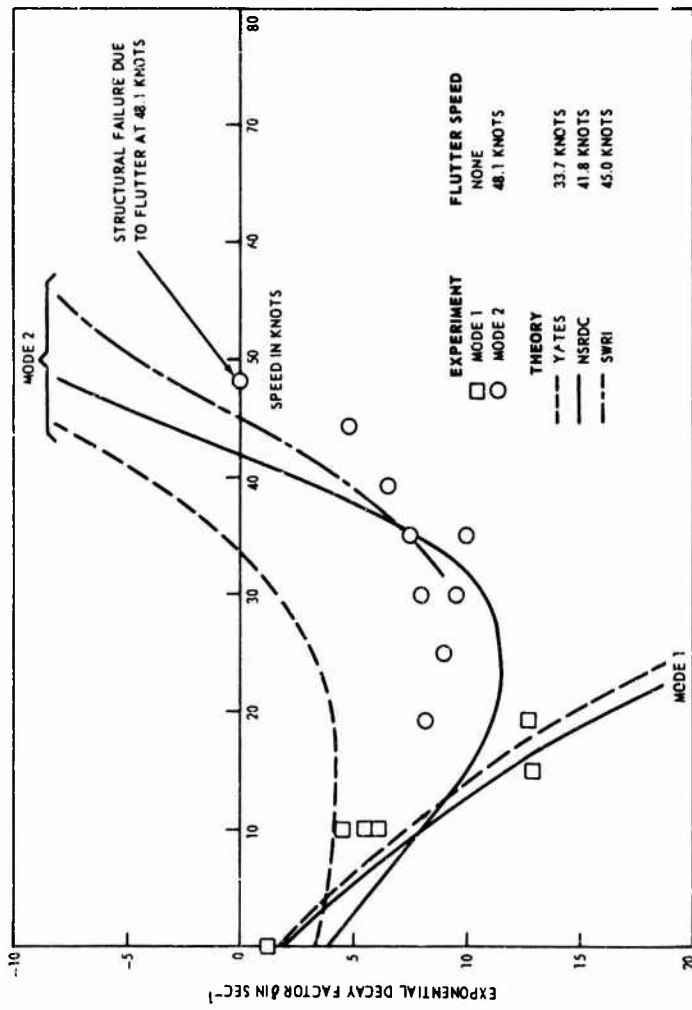


Figure 17 — Exponential Decay Factor δ as a Function of Speed for the SwRI 30-Inch Flutter Model

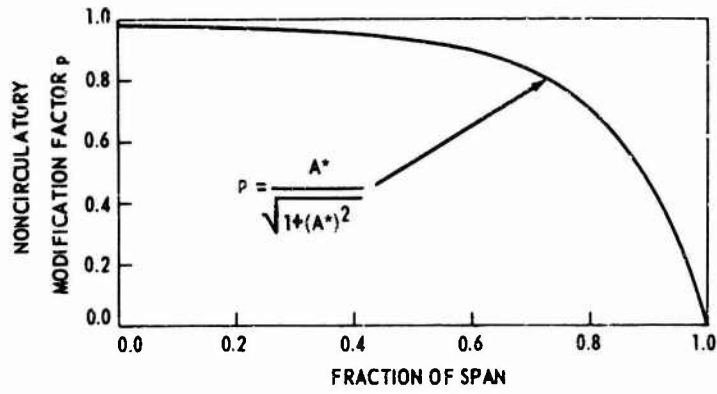


Figure 19 – Noncirculatory Modification Factor p as a Function of Spanwise Position for an Aspect Ratio 5 Hydrofoil

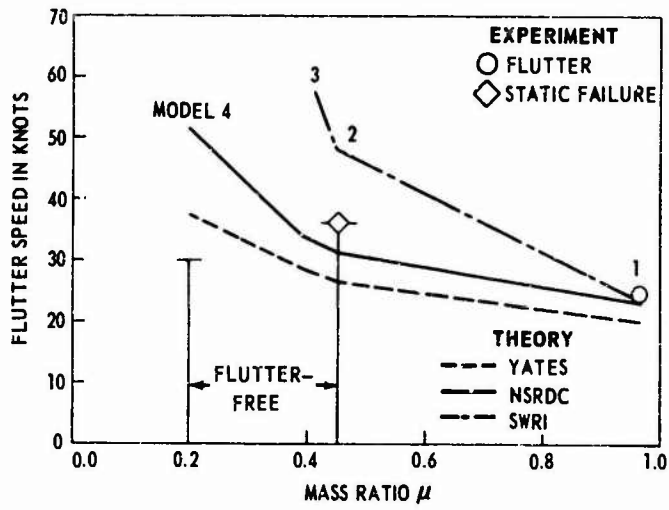


Figure 20 – Theoretical and Experimental Flutter Speeds for Models 1-4 as a Function of Mass Ratio

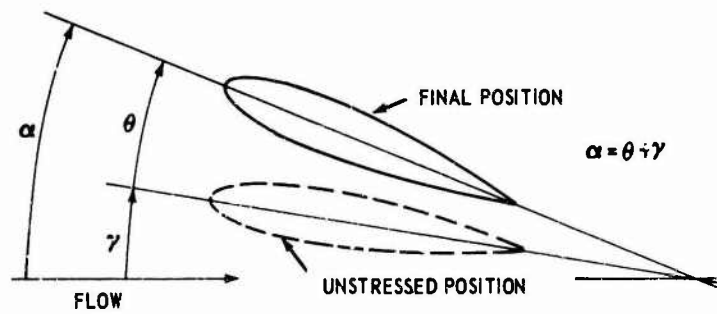


Figure 21 – Foil Deflection Angles

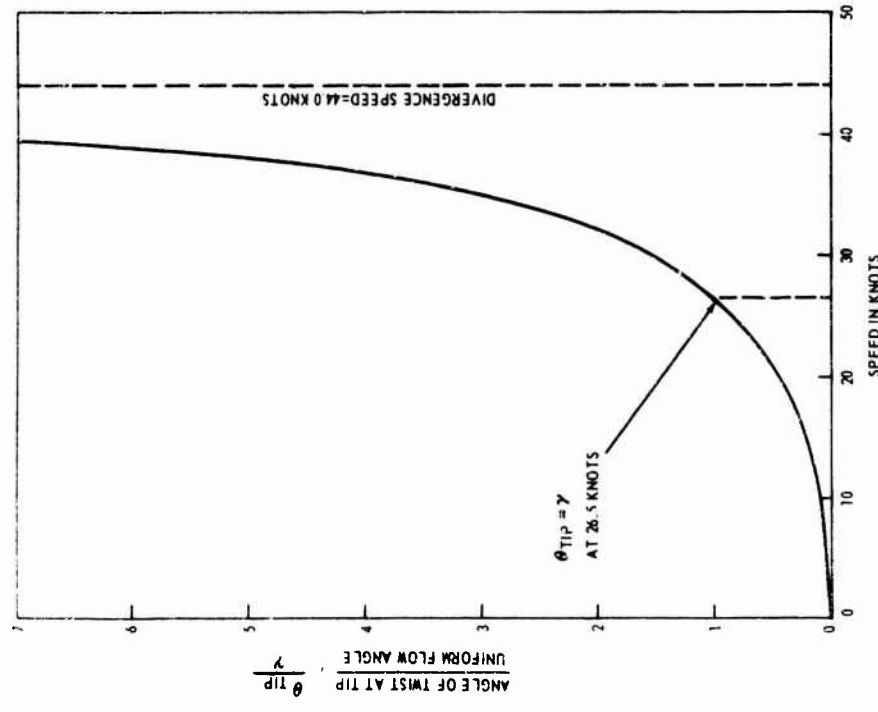


Figure 22 - Ratio of Angle of Twist at Tip to Uniform Misalignment Angle as a Function of Speed for Model 2

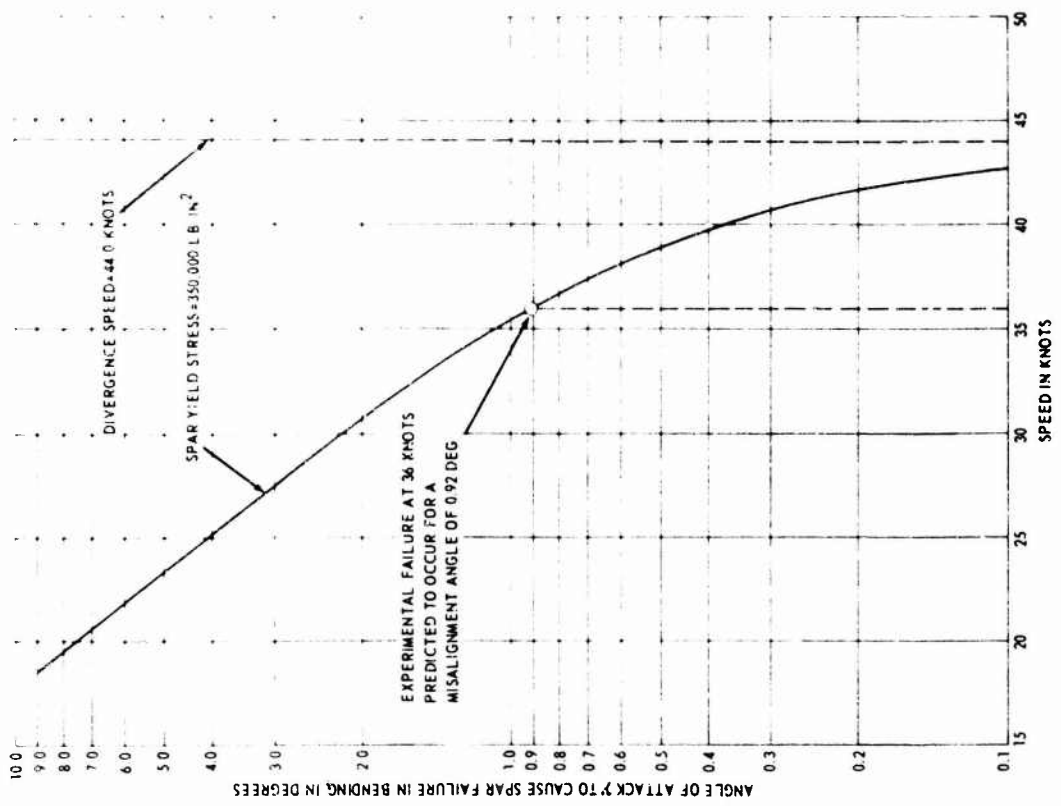


Figure 23 - Misalignment Angle γ to Cause Spar Failure in Bending for Model 2 as a Function of Speed

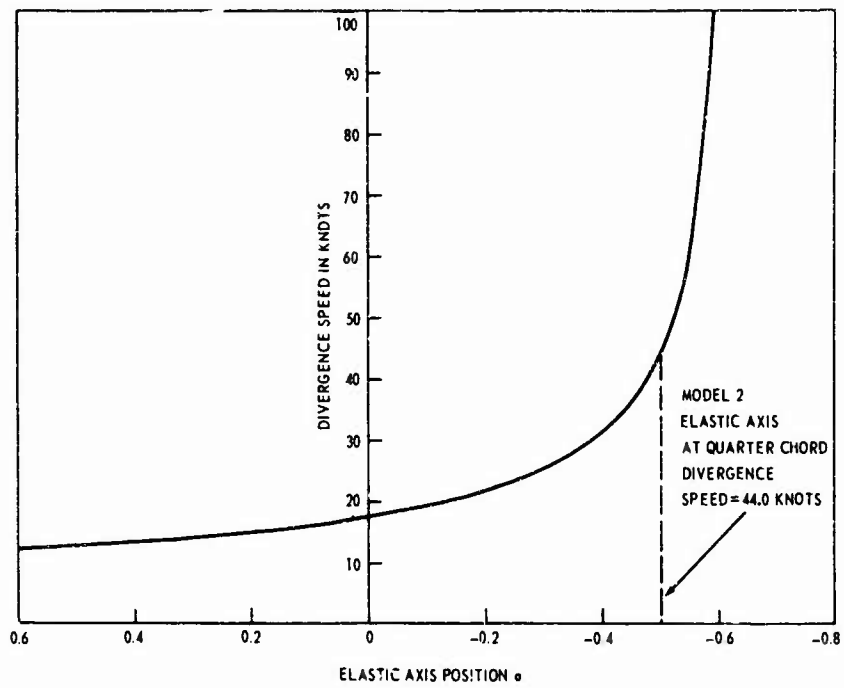


Figure 24 – Theoretical Divergence Speed as a Function of Elastic Axis Position for Model 2

TABLE 1

Structural Parameter Values for the Flutter Models

	SWRI 30-Inch Parent Model	Model 1	Model 2	Model 3	Model 4
μ	0.99	0.963	0.455	0.395	0.202
r_{α}	0.524	0.524	0.523	0.528	0.523
r_{α}^2	0.512	0.508	0.503	0.511	0.506
EI (lb-in. ²)	3.40×10^6	56,900	55,300	55,800	56,700
GJ (lb-in. ²)	0.973×10^6	19,200	16,420	16,440	15,630
L (in.)	30	15	15	15	15

TABLE 2

Theoretical and Experimental Natural Frequencies for SwRI 30-Inch Parent Model:

$$\mu = 0.93$$

Mode Number and Type <i>B</i> = Bending <i>T</i> = Torsion	Theoretical (in Vacuum)	Experimental (in Air)	Theoretical (in Water)		Experimental (in Water)
			Yates Hydrodynamics	NSRDC Hydrodynamics	
1 (1B, 1T)	10.07	9.63	7.17	8.03	7.3
2 (1T, 1B)	28.28	31.9	22.15	23.57	23.8
3 (2T, 1T, 2B, 1B)	50.17	—	37.51	39.96	—
4 (3T, 2T, 2B)	79.35	—	59.05	62.29	—
5 (4T, 3T, 2T, 2B)	116.7	—	87.90	92.18	—
6 (5T, 2T, 2B)	126.4	—	97.75	103.1	—

NOTE: All frequencies are given in Hertz.

TABLE 3

Theoretical and Experimental Natural Frequencies for Model 1

$\mu = 0.963$

Mode Number and Type <i>B</i> = Bending <i>T</i> = Torsion	Theoretical (in Vacuum)	Experimental (in Air)		Theoretical (in Water)		Experimental (in Water)
		Electro- magnetic Shaker	Tip Excitation	Yates Hydro- dynamics	NSRDC Hydro- dynamics	Tip Excitation
1 (1B, 1T)	10.78	11.1	11.0	7.59	8.19	8.4
2 (1T, 1B)	31.83	35.1	33	24.76	24.12	27
3 (2T, 1T, 2B, 1B)	55.68	58-61	-	51	41.12	-
4 (3T, 2T, 2B)	88.89	99.0	-	65.58	68.38	-
5 (4T, 3T, 2T, 2B) Vacuum (2T, 2B) Water	131.6	144.8	-	98.54	98.50	-
6 (5T, 2T, 2B) Vacuum (4T, 4B, 2B) Water	140.2	157.1	-	107.6	102.9	-

NOTE: All frequencies are given in Hertz.

TABLE 4

Theoretical and Experimental Natural Frequencies for Model 2

$\mu = 0.455$

Mode Number and Type <i>B</i> = Bending <i>T</i> = Torsion	Theoretical (in Vacuum)	Experimental (in Air)		Theoretical (in Water)		Experimental (in Water)
		Electro- magnetic Shaker	Tip Excitation	Yates Hydro- dynamics	NSRDC Hydro- dynamics	Tip Excitation
1 (1B, 1T)	15.30	15.7	15.6	8.63	10.18	9.9
2 (1T, 1B)	43.65	46.4	42	28.17	31.10	30
3 (2T, 1T, 2B, 1B)	77.03	79.8	-	46.59	51.68	-
4 (3T, 2T, 2B)	122.1	128.5	-	73.20	79.38	-
5 (4T, 3T, 2T, 2B)	180.0	181.3	-	109.7	117.9	-
6 (5T, 2T, 2B)	194.2	191.7	-	123.5	134.5	-

NOTE: All frequencies are given in Hertz.

Table 5
Theoretical and Experimental Natural Frequencies for Model 3
 $\mu = 0.395$

Mode Number and Type / Bending / Torsion	Theoretical (in Vacuum)	Experimental (in Air)		Theoretical (in Water)		Experimental (in Water)
		Electro- magnetic Shaker	Tip Excitation	Yates Hydro- dynamics	NSRDC Hydro- dynamics	Tip Excitation
1 (1B, 1T)	16.45	17.2	-	8.84	10.55	-
2 (1T, 1B)	46.69	49.2	-	28.95	32.37	-
3 (2T, 1T, 2B, 1B)	82.45	86.8	-	47.81	53.32	-
4 (3T, 2T, 2B)	130.4	142.0	-	74.97	81.90	-
5 (4T, 3T, 2T, 2B)	192.2	200.3	-	112.3	121.3	-
6 (5T, 2T, 2B)	208.2	214.5	-	127.0	140.5	-

NOTE: All frequencies are given in Hertz.

TABLE 6
Theoretical and Experimental Natural Frequencies for Model 4
 $\mu = 0.202$

Mode Number and Type / Bending / Torsion	Theoretical (in Vacuum)	Experimental (in Air)		Theoretical (in Water)		Experimental (in Water)
		Electro- magnetic Shaker	Tip Excitation	Yates Hydro- dynamics	NSRDC Hydro- dynamics	Tip Excitation
1 (1B, 1T)	23.04	22.5	-	9.57	11.77	-
2 (1T, 1B)	61.02	68.9	71	31.54	35.90	35
3 (2T, 1T, 2B, 1B)	108.4	105.9	-	51.89	59.67	-
4 (3T, 2T, 2B)	179.4	173.9	-	80.62	89.69	-
5 (4T, 2B) Vacuum (4T, 3T, 2T, 2B) Water	261.6	-	-	120.6	132.6	-
6 (3T, 2T, 1T, 2B) Vacuum (5T, 2T, 2B) Water	268.3	-	-	139.0	155.9	-

NOTE: All frequencies are given in Hertz.

TABLE 7
Measured Structural Damping ζ_s for Flutter Models

Model Number	1		2		3		4		Parent*	
Mode Number	1	2	1	2	1	2	1	2	1	2
Tip Excitation (Air)	0.0095	0.021	0.011	-	-	-	-	-	0.008	0.021
Tip Excitation (Water)	0.0099	0.024	0.018	0.033	-	-	-	0.052	0.035	0.024
Forced Oscillation (Air)	0.047	0.0045	0.024	0.010	0.024	0.010	0.036	0.0097	-	-

*Obtained from Reference 11.

REFERENCES

1. Baird, E. F. et. al., "Investigation of Hydrofoil Flutter - Final Report," Grumman Aircraft Engineering Corporation Report D-10-480.3 (Feb 1962).
2. Abramson, H. N. and Langner, C. G., "Correlation of Various Subcavitating Hydrofoil Flutter Predictions Using Modified Oscillatory Lift and Moment Coefficients," Southwest Research Institute, Contract N0bs-88599 (Jun 1964).
3. Rowe, W. S. and Marvin, T. G. B., "A Program of Theoretical Research on Hydroelastic stability," The Boeing Company, Contract N00014-67-C-0348 (Nov 1968).
4. Herr, R. W., "A Study of Flutter at Low Mass Ratio with Possible Application to Hydrofoils," NASA TN D-831 (May 1961).
5. Kaplan, P. and Lehman, A. F., "An Experimental Study of Hydroelastic Instabilities of Finite Span Hydrofoils under Cavitating Conditions, AIAA J. Aircraft, 3, 3, pp. 262-269 (May-Jun 1966).
6. Caporali, R. L. and Brunelle, E. J., "Hydrofoil Instability At Low Mass Density Ratios," Princeton University, Aerospace and Mechanical Sciences Report 670 (Mar 1964).
7. Yates, E. C., Jr., "Flutter Prediction at Low Mass-Density Ratios with Application to the Finite-Span Noncavitating Hydrofoil," AIAA Third Marine Systems and ASW Meeting (Apr-May 1968).
8. Abramson, H. N. and Ransleben, G. E., Jr., "An Experimental Investigation of Flutter of a Fully Submerged Subcavitating Hydrofoil," Southwest Research Institute, Contract Nonr-3335(00) (Dec 1963).
9. Ransleben, G. E., Jr., "Experimental Determination of Variation of Hydrofoil Flutter Speed with Mass Ratio," Southwest Research Institute, Contract N00014-69-C-0219 (Apr 1970).
10. Brownell, W. F. and Miller, M. L., "Hydromechanics Cavitation Research Facilities and Techniques in Use at the David Taylor Model Basin," Symposium on Cavitation Research Facilities and Techniques, American Society of Mechanical Engineers (May 1964); also David Taylor Model Basin Report 1856 (Oct 1964).
11. Chu, W.-H. and Abramson, H. N., "Further Calculations of the Flutter Speed of a Fully Submerged Subcavitating Hydrofoil," Southwest Research Institute Contract N00014-68-C-0259 (Jun 1968).
12. Timoshenko, S., "Strength of Materials," Part I, Third Edition, D. Van Nostrand Company, Princeton, New Jersey (1955), p. 150.
13. Bisplinghoff, R. L. et. al., "Aeroelasticity," Addison-Wesley Publishing Company, Cambridge Massachusetts (1955), p. 42.

14. Scanlan, R. H. and Rosenbaum, R., "Aircraft Vibration and Flutter," Dover Publications, Inc., New York (1968), pp. 87-88.
15. Peterson, Leonard, "Theoretical Basis for SADSAM III Computer Program," MacNeal Schwendler Corporation Project Report (May 1966).
16. Peterson, Leonard, "SADSAM III User's Manual," MacNeal Schwendler Corporation Project Report (May 1966).
17. Peterson, Leonard, "Description of SADSAM III Computer Program," MacNeal Schwendler Corporation Project Report (May 1966).
18. Abramson, H. N. et. al., "Hydroelasticity With Special Reference to Hydrofoil Craft," NSRDC Report 2557 (Sep 1967).
19. Huang, T. T., "Experimental Study of a Low Modulus Flutter Model for Strut-Foil-Pod Configurations," Hydronautics, Incorporated Technical Report 459-2 (Jul 1967).

UNCLASSIFIED

DOCUMENT CONTROL DATA - R & D		
<small>1. REPORT NUMBER (If the report is classified, this information must be entered when the overall report is classified)</small> Naval Ship Research and Development Center Washington, D. C. 20334		<small>2a. REPORT SECURITY CLASSIFICATION</small> UNCLASSIFIED
		<small>2b. GROUP</small>
<small>3. TITLE</small> FLUTTER AND DIVERGENCE CHARACTERISTICS OF FOUR LOW MASS RATIO HYDROFOILS		
<small>4. REPORT NOTES (Type of report and inclusive dates)</small> Final Report		
<small>5. AUTHOR(S) (First name, middle initial, last name)</small> Peter K. Beseh Yuan-Ning Lau		
<small>6. REPORT DATE</small> January 1971	<small>7a. TOTAL NO. OF PAGES</small> 19	<small>7b. NO. OF REFS</small> 19
<small>8a. CONTRACT OR GRANT NO.</small> S4606	<small>9a. ORIGINATOR'S REPORT NUMBER(S)</small> 3410	
<small>b. PROJECT NO.</small> Task 1703	<small>9b. OTHER REPORT NO(S) (Any other numbers that may be assigned this report)</small>	
<small>10. DISTRIBUTION STATEMENT</small> Approved for public release: Distribution Unlimited		
<small>11. SUPPLEMENTARY NOTES</small>		<small>12. SPONSORING MILITARY ACTIVITY</small> Naval Ship Systems Command Washington, D. C. 20360
<small>13. ABSTRACT</small> <p>Four low mass ratio hydrofoil models of aspect ratio 5 were flutter tested. The flutter speed of the mass ratio 0.963 model was 24.7 knots. The other three models, of mass ratios 0.455, 0.395, and 0.202, were subject to static failure in bending at about 36 knots and did not flutter below this speed. The results were compared with the predictions of three flutter theories. All theories gave conservative flutter speed predictions at mass ratio 0.963. Two of the theories were also conservative at mass ratio 0.455. The other predictions could not be evaluated. Model divergence characteristics were responsible for model failure in bending.</p>		

DD FORM 1473 (PAGE 1)
 1 NOV 65
 S/N 0101-807-6801

UNCLASSIFIED
 Security Classification

UNCLASSIFIED

Security Classification

14 KEY WORDS	LINK A		LINK B		LINK C	
	ROLE	WT	ROLE	WT	ROLE	WT
Aspect ratio Hydrofoil Flutter Divergence characteristics						

UNCLASSIFIED

Security Classification